NREL/TP-411-6612 • UC Category: 271 • DE94011815

Small-Angle X-Ray Scattering Studies of Microvoids in Amorphous Silicon-Based Semiconductors

Annual Subcontract Report
1 February 1992 – 31 January 1993

D. L. Williamson, S. J. Jones, Y. Chen
Colorado School of Mines
Golden, Colorado

NREL technical monitor: A. H. Mahan

National Renewable Energy Laboratory
1617 Cole Boulevard
Golden, Colorado 80401-3393
A national laboratory of the U.S. Department of Energy
Operated by Midwest Research Institute
for the U.S. Department of Energy
under contract No. DE-AC02-83CH10093

Prepared under Subcontract No. XG-1-10063-3

June 1994

MASTER

DISTRIBUTION OF THIS DOCUMENT IS UNLIMITED

NOTICE

NOTICE: This report was prepared as an account of work sponsored by an agency of the United States government. Neither the United States government nor any agency thereof, nor any of their employees, makes any warranty, express or implied, or assumes any legal liability or responsibility for the accuracy, completeness, or usefulness of any information, apparatus, product, or process disclosed, or represents that its use would not infringe privately owned rights. Reference herein to any specific commercial product, process, or service by trade name, trademark, manufacturer, or otherwise does not necessarily constitute or imply its endorsement, recommendation, or favoring by the United States government or any agency thereof. The views and opinions of authors expressed herein do not necessarily state or reflect those of the United States government or any agency thereof.

Printed in the United States of America
Available from:
National Technical Information Service
U.S. Department of Commerce
5285 Port Royal Road
Springfield, VA 22161

Price: Microfiche A01
Printed Copy A03

Codes are used for pricing all publications. The code is determined by the number of pages in the publication. Information pertaining to the pricing codes can be found in the current issue of the following publications which are generally available in most libraries: *Energy Research Abstracts (ERA)*; *Government Reports Announcements and Index (GRA and I)*; *Scientific and Technical Abstract Reports (STAR)*; and publication NTIS-PR-360 available from NTIS at the above address.

Printed on recycled paper

DISCLAIMER

Portions of this document may be illegible electronic image products. Images are produced from the best available original document.

1. SUMMARY

1.1 OBJECTIVES

Our general objectives are to provide new details of the microstructure for the size scale from about 1 to 30 nm in high-quality a-Si:H and related alloys prepared by current state-of-the-art deposition methods as well as by new and emerging deposition technologies and thereby help determine the role of microvoids and other density fluctuations in controlling the opto-electronic properties.

More specifically, the objectives are to determine whether the presence of microstructure as detected by small-angle x-ray scattering (SAXS) (1) limits the photovoltaic properties of device-quality a-Si:H, (2) plays a role in determining the photo-stability of a-Si:H, and (3) is responsible for degradation of the photovoltaic properties due to alloying with Ge, C and other constituents. The approach involves collaboration with several groups that can supply relevant systematic sets of samples and the associated opto-electronic data to help address these issues. Since the SAXS technique has not been a standard characterization technique for thin-film materials, and was recently set up at CSM with support by NREL, the project involves considerable development of the method with regard to standardizing the procedures, minimizing substrate influences and implementing improved data reduction and modeling methodology. Precise, highly reproducible, and accurate results are being sought in order to allow useful, reliable, and sensitive comparisons of materials deposited under different conditions, by different methods, and by different systems that represent the same nominal method.

1.2 RESEARCH OVERVIEW

1.2.1 Device-Quality a-Si:H

During this second year of NREL support we have made SAXS and flotation density measurements of numerous a-Si:H thin films prepared by rf glow-discharge (PECVD), reactive dc magnetron sputtering (RMS), amd electron cyclotron resonance (ECR). Several of these samples can be characterized as "device quality" on the basis of their photoresponse and other opto-electronic properties. Deposition variables of particlar interest were the effects of plasma power (primarily to change deposition rate), of various diluting gases (H_2, Ar, He, and Xe), and of higher substrate temperatures. Suppliers of a-Si:H films produced by the various deposition methods included: PECVD - USSC, Ecole Polytechnique (Paris), and IACS(Calcutta); high-frequency PECVD - Univ. Neuchatel; RMS - U. Illinois; and ECR - JPL.

A correlation of SAXS-determined microstructure and solar cell behavior has been obtained for the first time. A series of SAXS samples and solar cells were prepared by USSC with different deposition rates used for growth of the i-layer. This was done by adjusting the rf power of the glow-discharge plasma. The increased microstructure in the form of microvoids about 1 nm in diameter correlated with degraded solar cell efficiencies. The increased microstructure was shown not to be associated with a columnar-like microstructure. In addition, it was found that the solar cells with i-layers having the increased microvoid contents degraded more rapidly under light soaking for 600 hours. Details of this study have been published [1].

Several of the other a-Si:H samples produced by the various methods and under certain conditions showed a significant amount of SAXS-determined microstructure that correlated systematically with deposition variables and degraded opto-electronic behavior. In two cases (ECR and RMS) a significant amount of microstucture was present and yet photo/dark conductivity ratios typical of device-quality material were obtained. However, neither of these materials have been incorporated as the i-layer into a solar cell.

1.2.2 Alloys

Several sets of a-SiGe:H alloys from various groups have been analyzed. These include PECVD films from NREL, Solarex, USSC, Stuttgart University, IACS (Calcutta), and Princeton University. The latter samples were prepared with GeF_4 rather than GeH_4.

A systematic series of 10 samples from Stuttgart University with Ge contents from 0 to 37 at.% provide strong evidence for a direct link between the SAXS-determined microstructure and opto-electronic degradation. Above about 20 at.% Ge a sharp transition in the microstructure occurs consistent with a change to columnar-like growth. Above this same composition the photo/dark conductivity ratio and the defect density determined by PDS show significant decreases and increases, respectively. Details of this study have recently been submitted for publication [2].

Alloys from NREL and Solarex containing from 40 to 70 at.%Ge were found to have strong SAXS signals and columnar microstructure [3]. Flotation densities yielded a typical density deficit of 6%, consistent with an interpretation of voids or low density, H-rich regions as the source of the SAXS. Japanese researchers have been suggesting that alloy segregation (Ge-clusters) is the origin of the SAXS in a-SiGe:H alloys [4,5]. Additional evidence that Ge clustering is not responsible for the SAXS comes from measurements of several a-Ge:H films prepared by PECVD at Harvard. The SAXS

signals are similar to those from the alloys. The effects of electrode spacing and rf power have been examined and although significant reductions in the SAXS can be obtained, clear evidence of columnar-like microstructure remains in the best opto-electronic-quality a-Ge:H available to date.

The USSC series (19, 31, 41 at.%Ge) shows a similar trend to that of the Stuttgart series in that enhanced columnar-like microstructure appears for the 31 and 41% Ge films, although the magnitudes of the increases are not as great. Solar cells containing i-layers made under identical deposition parameters used for the SAXS samples show reduced initial efficiencies with increasing Ge. Additional experiments with lower Ge contents and other deposition conditions are underway and will be reported at the MRS Spring meeting.

The a-SiGe:H films from IACS are quite similar to the PECVD films from the other groups based on the SAXS results while the Princeton material, prepared with GeF_4, suggests a significantly different size distribution of scattering centers and a reduced tendency for columnar-like microstructure.

A series of a-SiC:H films prepared by reactive dc magnetron sputtering (U. Illinois) shows SAXS behavior consistent with columnar-like microstructure [6], in contrast to earlier results from PECVD material from NREL which showed no oriented microstrucure [7].

1.2.3 SAXS Methodology and Analysis

An experimental problem with the SAXS apparatus was discovered in June, 1992, during a careful examination and adjustment of the system alignment. The cause of the problem was a design flaw in the commercial SAXS system obtained for our research. The flaw was quickly repaired and a systematic study of the effect of the flaw on previous SAXS data was made and reported to NREL. The effect of the flaw was to produce an apparent decrease in the SAXS signal with increasing angle above a certain angle. This effect therefore caused errors in the shape of the SAXS curves above this angle. The errors in void fractions and size distributions were relatively small for all samples showing relatively strong SAXS corresponding to void fractions above about 2 volume %, while those for the more weakly scattering material (typically device-quality PECVD films) were larger. The reanalyzed size distributions of the latter type of samples show significantly smaller fractions of the very small voids (about 1 nm diameter), a slight shift in their size toward 2 nm, and a corresponding increase in the fractional contribution from larger scattering centers (about 2 to 3 nm diameter).

A new feature in most of the SAXS curves that was detected after repair of the

flaw is an angle-independent behavior at the larger angles. In addition, for some of the weakest scattering samples, a slight increase in SAXS with increasing angle at the largest angles was found. Possible physical explanations for these observations have been considered and verified with several experiments. The most important effect that has come to light is that due to random alloy scattering (Laue monotonic scattering) and it is quite significant for the a-SiGe:H alloys. This effect also produces an observable contribution due to H alloying in a-Si:H.

Where appropriate, corrections to previously published SAXS data and interpretations will be reported in the open literature. All samples still available are being remeasured in preparation for these corrections.

A study of the possible interdiffusion between the SAXS Al-foil substrate and a-Si:H or a-Ge:H films has been completed. The temperature at which significant interdiffusion occurs for the Al/a-Si:H and Al/a-Ge:H interfaces is 450°C. An oxide layer about 10 nm thick on the Al-foil substrates is apparently serving as an effective diffusion barrier until this temperature is reached.

Progress has been made in the modeling of the anisotropic SAXS that is observed by tilting a sample relative to the x-ray beam. Assuming ellipsoidal-shaped voids, values of the aspect ratio of the axes can be adjusted for up to five distinct sizes of voids in order to fit two or more sets of SAXS curves obtained for different tilt angles.

1.3 CONCLUSIONS

The SAXS technique is able to provide microstructural information not available from other methods and with a high degree of sensitivity. It is particularly sensitive to microvoids and the presence of oriented microstructure. The latter is readily associated with columnar-type growth and can even be observed in premature stages not detectable by TEM. Specific conclusions from our second year of work under NREL support are as follows:

(a) a-Si:H p-i-n solar cells that contain more microstructure in the i-layer in the form of very small voids show lower initial efficiencies and more light-induced degradation.

(b) a-$Si_{1-x}Ge_x$:H alloys that show a microstructural transition corresponding to enhanced columnar-like growth above x=0.2 have corresponding sharp degradations in opto-electronic properties above this same Ge content. This provides strong evidence that the increased low-density heterogeniety is directly responsible for the degradation.

(c) Dilution during PECVD growth with Ar or He causes enhanced microstructure in the form of microvoids. The Ar-diluted material shows columnar-like growth while the

He-diluted material shows no preferred orientation in the microstructure. A correlated opto-electronic degradation in the material made under increasing Ar dilution occurs. Although several ECR-produced films were made with and without Xe dilution, too many other parameters were varied to allow a conclusion on the effect of the Xe. The ECR films are unique in that they show evidence of disc-like microvoids.

(d) Both the ECR and RMS a-Si:H films show that high photo/dark conductivity ratios ($\sim 10^5$) and significant microvoid volume fractions (3-8%) can coexist, however solar cells have not yet been fabricated with these alternate deposition methods.

(e) Flotation densities of a-$Si_{1-x}Ge_x$:H alloys for x up to 0.57 show a systematically increasing density deficit (reaching 9%) compared to crystalline densities for samples prepared in 5 different PECVD systems. Coexistence of Ge-rich or Si-rich regions in these films cannot yet be ruled out however the evidence presented here strongly supports the void (or low density H-rich region) interpretation. There are differences in the degree of oriented-type microstructure for a similar x in films from different systems.

(f) Solar cells made from a-$Si_{1-x}Ge_x$:H alloys with x=0.19, 0.30, and 0.41 have efficiencies that decrease with increasing x and SAXS from the corresponding alloys shows enhanced microstructure for x=0.30 and 0.41.

(g) a-$Si_{1-x}Ge_x$:H:F alloys prepared from silane and germanium fluoride at Princeton are microstructurally different from all the other PECVD alloys in that a larger fraction of smaller scattering centers are present in a more randomly oriented array.

(h) Correlations exists between the SAXS-determined microstructures of a-Ge:H films and the opto-electronic properties for variable electrode spacing and variable plasma power. a-Ge:H without oriented microstructure has not yet been observed.

(i) a-SiC:H alloys prepared by RMS all have columnar-like microstructure in contrast with earlier PECVD materials which had randomly oriented or spherical microvoids.

(j) Angle-independent, random alloy scattering from a-$Si_{1-x}Ge_x$:H alloys has been observed and identified for the first time. A theoretical quadratic x dependence is in good agreement with the data. Effects due to random H alloying in the amorphous matrix of a-Si:H have also been observed. It is crucial to correct for this angle-independent effect in analyzing the SAXS data for microvoid contents.

(k) Interdiffusion is negligible between the aluminum foil substrate (used to prepare the films for SAXS) and the a-Si:H provided substrate temperatures are below 450°C.

(l) Modeling of the sample tilting effects on the SAXS intensities due to oriented scattering centers is possible on the basis of a distribution of ellipsoidal voids.

TABLE OF CONTENTS

	page
1. SUMMARY	3
1.1 Objectives	3
1.2 Research Overview	3
1.3 Conclusions	6
LIST OF FIGURES	9
LIST OF TABLES	11
2. INTRODUCTION	12
3. STUDIES OF a-Si:H	14
3.1 USSC Solar Cell/SAXS Correlation	14
3.2 VHF-PECVD Ar Dilution	16
3.3 PECVD He Dilution	18
3.4 ECR Xe Dilution and Other Variables	20
3.5 RMS a-Si:H	23
3.6 IACS Material	26
4. ALLOYS	27
4.1 a-SiGe:H Microstructure Transition	27
4.2 Comparison of PECVD Films from Several Groups	31
4.2.1 Laue monotonic effect	31
4.2.2 Integrated SAXS and tilting effects	34
4.2.3 Flotation densities	36
4.3 RMS a-SiC:H	37
5. STUDIES OF a-Ge:H	38
5.1 Electrode Spacing Study	38
5.2 Plasma Power Study	40
6. DATA ANALYSIS AND MODELING	42
6.1 Modified Analysis Procedures	42
6.2 Modeling Progress	43
7. INTERDIFFUSION STUDY	46
8. FUTURE STUDIES	47
9. ACKNOWLEDGEMENTS	47
10. REFERENCES	47

LIST OF FIGURES page

1. SAXS data for USSC a-Si:H films grown at different deposition rates. 15

2. SAXS data for USSC a-Si:H film grown at 1.35 nm/s in two orientations relative to the x-ray beam. 15

3. Initial and light-degraded efficiencies of a-Si:H p-i-n solar cells as a function of i-layer deposition rate. 15

4. SAXS from a-Si:H deposited by VHF-PECVD with different Ar dilutions. 17

5. SAXS versus substrate temperature for a-Si:H prepared without H dilution. 19

6. SAXS from several ECR-produced a-Si:H films. 20

7. SAXS from RMS a-Si:H films prepared with different H_2 partial pressures. 23

8. SAXS from RMS a-Si:H films deposited at higher temperatures. 25

9. SAXS data for IACS a-Si:H. 26

10. SAXS data for a-SiGe:H films. 27

11. Variations in Q, defect density, and photo/dark conductivity ratios. 28

12. Effect of tilting on SAXS intensity for two Ge contents. 29

13. Flotation density results compared with crystalline densities vs Ge content. 30

14. Experimentally determined background signals from a-SiGe:H alloys 33

15. Theoretical Laue monotonic scattering contribution for a-SiGe:H and a-SiC:H alloys of various H contents. 33

16. SAXS Q-values versus Ge content for a-SiGe:H alloys from several groups. 34

17. Tilting effect ratio versus Ge content for a-SiGe:H films from several groups. 35

18. Fraction of scattering centers that have a minor axis diameter between 3 and 4 nm based on size distribution fitting of SAXS data from non-tilted a-SiGe:H alloys. 36

19. Flotation density results from a-SiGe:H alloys compared to crystalline density of SiGe alloys based on Vegard's law. 36

20. SAXS from a-SiC:H alloys prepared by RMS. 37

21. SAXS data from a-Ge:H films prepared at different electrode spacings. 39

22. I x h plots of SAXS data from a-Ge:H films prepared simultaneously on Al-foil and c-Si substrates. 40

23. SAXS data from a-Ge:H films prepared with different rf plasma powers. 41

24. Theoretical contribution to SAXS intensity due to incoherent Compton scattering and thermal-diffuse scattering for Al and Si. 42

25. Experimental and theoretical contributions to SAXS intensity due to thermal-diffuse scattering effect. 43

26. Comparison of SAXS data from a-Ge:H film with theoretical modelling curves based upon a distribution of ellipsoidal voids. 45

LIST OF TABLES page

1. 1992-93 list of collaborators and nature of samples submitted. 13

2. Material properties and cell performance for USSC i-layers prepared at two different deposition rates. 16

3. SAXS and opto-electronic data from VHF-PECVD a-Si:H films with different Ar dilutions. 17

4. Deposition conditions, SAXS Q-values, and opto-electronic properties of a-Si:H prepared with and without He dilution. 19

5. Deposition parameters used for the ECR-produced films. 21

6. SAXS, flotation density, and opto-electronic data for the ECR-produced films. 22

7. RMS film preparation conditions, thicknesses, SAXS and flotation results. 24

8. RMS a-Si:H films, substrate temperatures, SAXS and flotation results. 25

9. Deposition conditions and SAXS results for IACS a-Si:H films. 26

10. SAXS and flotation density results for a-SiGe:H alloys from several groups. 32

11. SAXS data from RMS a-SiC:H films. 38

12. Deposition conditions, opto-electronic data and SAXS results for a-Ge:H films. 38

13. Fit parameters for the theoretical curves shown in Figure 26. 46

2. INTRODUCTION

Direct evidence of microvoids and other extended-defects that produce density fluctuations in a material can be obtained from small-angle scattering of x-rays, neutrons, or electrons. Inversion of the scattered intensity versus angle leads to direct information on the size and shape of the density fluctuations and the magnitude of the scattered intensity can provide quantitative information on the volume fraction of the microstructural component that produces the observed small-angle scattering [8,9]. This research project takes advantage of such abilities of small-angle x-ray scattering (SAXS) applied to thin films of a-Si:H and related alloys. Some of the first experiments at the Colorado School of Mines with NREL-produced material showed the systematic development of increased fractions of microvoids in correlation with substrate temperature [7] and with C alloying [7,10], and demonstrated detectable SAXS in device-quality material [11,12]. The latter has recently been confirmed by another group [5]. The origin of the SAXS from the PECVD device-quality a-Si:H material is not yet clearly established due to its very weak nature. We have also presented evidence for significant differences in the microstructure of high quality a-Si:H prepared by different methods [13].

Table 1 lists the groups that have submitted samples for SAXS characterization during the second year of NREL support, the deposition method, and the primary deposition variables for each set of samples. The number of samples submitted by each group is also listed. Our first annual report provided a detailed description of our experimental SAXS set-up, the geometrical requirements for samples, an overview of the data collection and reduction procedures, the flotation density measurement procedure, and the use of synchrotron SAXS facilities.

We discuss in section 3 the results from a-Si:H prepared with different methods and different conditions. Of particular importance is a correlation of the SAXS with photovoltaic properties. Section 4 presents extensive new results from a-SiGe:H alloys prepared by several groups. An important finding from one systematic set of alloys is a clear transition to a more heterogeneous microstructure upon varying only the Ge content. A detailed treatment of the Laue monotonic scattering effect is included together with convincing experimental evidence from the a-SiGe:H alloys. This section also includes a few results from RMS-prepared a-SiC:H alloys. Section 5 describes several new results from a-Ge:H films. Progress in our analytical modeling and data treatment methods is discussed in section 6. Results of an interdiffusion study with our high purity SAXS Al-foil are summarized in section 7. Experiments planned in the immediate future are indicated in section 8.

Table 1. 1992-93 List of Collaborators and nature of samples submitted

Institution/Company (Contact(s))	Sample Type (number)	Deposition Method	Primary Variable
USSC (Guha)	a-Si:H (3)	PECVD	rf power
	a-SiGe:H (6)	PECVD	Ge content
Univ. Illinois (Abelson/Yang)	a-Si:H (13)	Reactive dc magnetron sputtering (RMS)	H-content and higher T_s
	a-SiC:H (4)	RMS	C-content
Stuttgart U. (Bauer/Zedlitz)	a-SiGe:H (11)	PECVD	Ge content
Princeton U. (Wagner/Morin/Vasanth)	a-SiGe:H (5)	PECVD (GeF_4)	Ge content
JPL (Shing)	a-Si:H (7)	Electron-cyclotron-resonance (ECR)	Several variables and Xe dilution
Harvard (Paul/Wickbolt)	a-Ge:H (6)	PECVD	electrode spacing, rf power and substr. type
Neuchatel (Kroll)	a-Si:H (5)	High-freq. PECVD (70 MHz)	Ar dilution
Ecole Poly (Cabarrocas)	a-Si:H (6)	PECVD	He dilution and T_s
IACS (India) (Dusane/Ray) (via Crandall)	a-Si:H (5)	PECVD	Cathode T and H_2 dilution
	a-SiGe:H (12)	PECVD	Ge content and H_2 dilution

3. STUDIES of a-Si:H

3.1 USSC solar cell/SAXS correlation

Single-junction p-i-n solar cells were grown at USSC by the rf glow-discharge technique (PECVD) on stainless steel substrates kept at 300°C. Details of the deposition parameters are given elsewhere [14]. The intrinsic layers were grown using a disilane-hydrogen mixture and the dilution of the mixture and the rf power density were changed to obtain deposition rates between 0.14 and 1.4 nm/s. The thickness of the i layers was kept contant near 420 nm. The deposition conditions for the doped layers were kept constant for all the devices. The top contact was made using thermally evaporated ITO. Cell performance was measured under global AM1.5, red, and blue illumination.

Samples consisting of only the i layer, typically 1-μm thick, were deposited on 10-μm thick Al foil (99.999% pure) for the SAXS measurements and on c-Si wafers for IR measurements. The deposition conditions were nominally identical to those used to produce the solar cells.

Figure 1 shows the SAXS data for three films prepared at different deposition rates compared to those from a 70-μm c-Si wafer. There is a clear systematic increase in the SAXS with increased deposition rate. The nearly angle-independent SAXS above 2 nm^{-1} is attributed to the Laue monotonic effect as described later in section 4.2.1. After correcting for this contribution we estimate the volume fraction of voids, assuming a two phase system of voids+matrix, to be $1 \pm 0.5\%$ for the samples prepared with 0.14 and 0.62 nm/s deposition rates and $4 \pm 1\%$ for the one deposited at 1.35 nm/s. Figure 2 shows that upon tilting the latter sample, no significant change in the SAXS occured and this is consistent with spherical voids or randomly oriented non-spheres.

Assuming spherical voids, the sample with the larger void fraction was analyzed with a size distribution model and it was found that about 80% of the voids have a diameter near 0.9 nm and the remainder are mostly less than 10 nm in diameter. The very small voids account for most if not all of the increase in the volume fraction of voids compared to the two films prepared at the lower deposition rates.

The initial and light-degraded (after 600 h, one-sun, 50°C, open-circuit condition illumination) performances of the solar cells are shown in Fig. 3 as a function of the i-layer deposition rate. The solid lines suggest the systematic trends: both initial and light-degraded efficiencies decrease with increased deposition rate such that the relative degradation is about 13% for the intitial efficiencies and about 43% for the light-degraded efficiencies. Thus, the correlation of SAXS and cell efficiency indicates a degradation in solar cells with more microstructure in the i-layer. These results do not

support the suggestion by Matsuda et al. [15] that material with increased microstructure may be more stable. Their conclusion was based on photoconductivity measurements of materials deposited from Xe-diluted silane mixtures. Their observed dangling bond density, however, was found to be higher for films with poorer microstructure.

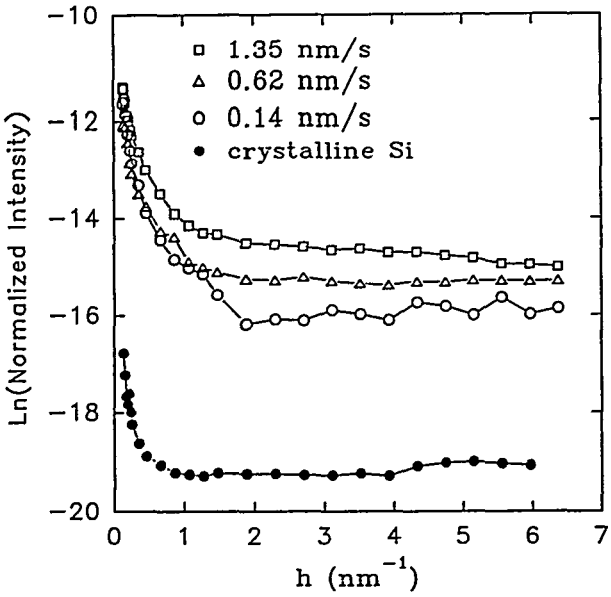

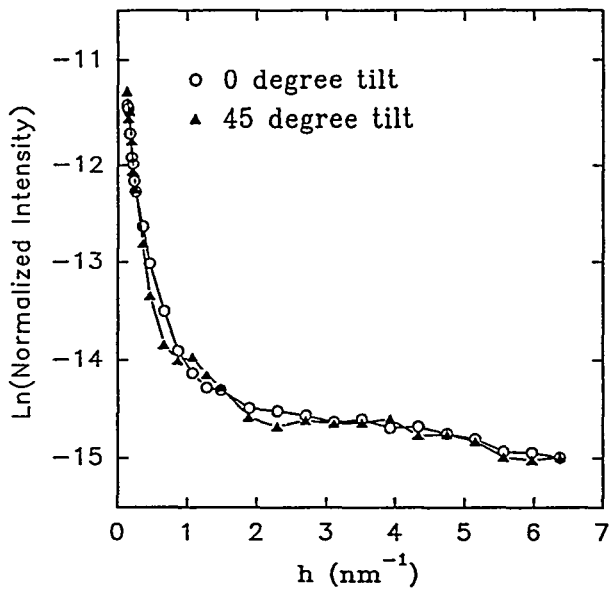

Fig. 1. (left) SAXS data for a-Si:H films grown at different deposition rates compared to data from c-Si. The intensity has been normalized and corrected for substrate effects according to the procedure in ref. 10. $h=4\pi\sin\theta/\lambda$, where λ is the x-ray wavelength (0.154 nm) and 2θ is the scattering angle.

Fig. 2. (right) SAXS data from the sample grown at 1.35 nm/s mounted in two orientations relative to the x-ray beam.

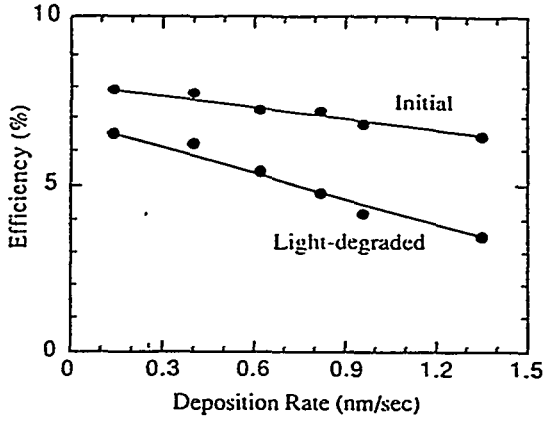

Fig. 3. Initial and light-degraded efficiencies of a-Si:H solar cells as a function of i-layer deposition rate.

Material properties and cell performance are compared in Table 2 for the lowest and highest deposition rates. Additional discussion of this experiment and these data can be found in ref. 1. The conclusion is that we see a correlation between microstructure determined by SAXS and IR and solar cell efficiencies and stabilities: with increasing microvoid density and microstruture fraction, both the initial and light-degraded solar cell performance are found to deteriorate.

Table 2. Material properties and cell performance for USSC samples prepared at two deposition rates.

Deposition rate	0.14 nm/s	1.35 nm/s
Void fraction	1 %	4 %
Predominant void diameter	---	0.9 nm
Hydrogen content	8 %	12 %
Microstructure fraction	8.4 %	18.4 %
$C_H(2000)$	6.4 %	6.3 %
Initial efficiency	7.85 %	6.31 %
Degraded efficiency	6.53 %	3.5 %
Initial red fill factor	0.67	0.52
Degraded red fill factor	0.52	0.43
Initial blue fill factor	0.73	0.67
Degraded blue fill factor	0.67	0.40

3.2 VHF-PECVD Ar dilution

A series of five films produced at Neuchatel University using the VHF (70 MHz) -PECVD technique [16] with different Ar to Silane gas mixtures has been investigated. Two films were prepared using no Ar dilution while three others were made with $SiH_4/Ar+SiH_4$ ratios of 0.41, 0.11 and 0.06. Details of several properties of similarly prepared films have recently been reported [17].

The SAXS was found to increase with decreasing silane fractions in the plasma as shown in Fig. 4. The integrated SAXS intensities ($\int Ihdh \equiv Q$, area under curve in Fig. 4b-type of plot) increased by a factor of 24 as the silane fraction decreased from 100% to 6%. Table 3 compares the changes in Q with variations in the opto-electronic properties, most of which were obtained by interpolations of data from ref. 17. Degradations indicated by the photo/dark conductivity ratio, the Urbach edge, sub-bandgap absorption (via PDS) and the light induced defects, all correlate with the decrease in silane fraction below 40% and the sharply increased microstructure detected by SAXS.

The reduced stability of the more defective material is consistent with the findings described above for the USSC film containing more microvoids.

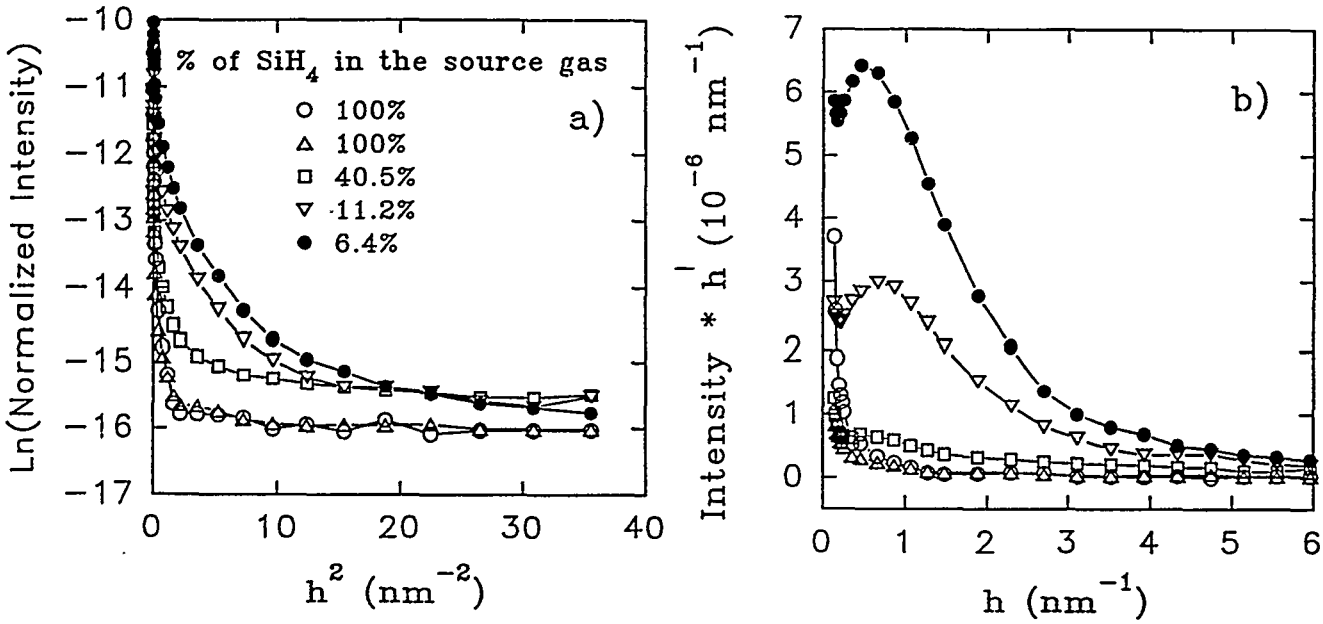

Fig. 4. SAXS from a-Si:H deposited by VHF-PECVD with different Ar dilutions.
a) Guinier plots; b) I x h plots

Table 3. SAXS and opto-electronic data from VHF-PECVD a-Si:H films with different Ar dilutions.

Sample	% SiH_4 in Ar	Q_{SAXS} (nm^{-2})	Q_0/Q_{45}	$\sigma_{photo}/\sigma_{dark}$	E_0 PDS (meV)	R	N_d PDS (cm^{-3})	$(\Delta N_d)_{illum}$ PDS (cm^{-3})
220192	100	4.9×10^{-7}	0.89	1.7×10^{6}	48	0.35	$\sim6\times10^{16}$	$\sim5\times10^{17}$
200192	100	7.1×10^{-7}	-	1.7×10^{6}	48	0.35	$\sim6\times10^{16}$	$\sim5\times10^{17}$
160192	40.5	1.8×10^{-6}	-	7.6×10^{5}	51	0.26	$\sim6\times10^{16}$	$\sim4\times10^{17}$
150192	11.2	6.5×10^{-6}	1.85	1.5×10^{5}	55	0.18	$\sim8\times10^{16}$	$\sim8\times10^{17}$
170192	6.4	1.2×10^{-5}	2.27	3.1×10^{4}	56	0.29	$\sim2\times10^{17}$	$\sim2\times10^{18}$

Three of the films were measured at a 45 degree tilt. The data from a sample produced with 100% silane were very similar to those from the sample in the non-tilted orientation showing that the scattering centers are either spherical or randomly oriented non-spheres. However, the SAXS at small h for the 11 and 6% silane fractions were much smaller than those from the non-tilted samples. Note the Q-ratios in Table 3. This clearly demonstrates that the increase in Q with increasing Ar dilution of the plasma is due to the formation of preferentially oriented, non-spherical scattering centers, probably due to columnar-like growth. Size distribution fitting of the data suggest a predominant minor-axis size of about 3 nm.

3.3 PECVD He dilution

Six films prepared at Ecole Polytechnique (Paris) using PECVD have been examined. Three of the films were made at different substrate temperatures using an undiluted silane plasma while the other three were produced in a 40% silane -60% He mixture (see Table 4). As shown in Fig. 5 for the films made with 100% silane, the SAXS decreases with increasing substrate temperature as we have typically observed in the past [7]. An important difference, however, is the much smaller SAXS from the film deposited at 100°C. Also in the past, SAXS from such low-temperature-deposited films shows the presence of columnar-like microstructure since the SAXS is sample-orientation dependent [7]. In this study, the tilt angle affects the SAXS for the 50°C film but not for the 100°C film, suggesting that for the latter film the scatterers are randomly oriented or spherical in shape. This lack of columnar-like growth may be related to the relatively low deposition rate (see Table 4).

As can be seen from the Q-values in Table 4 for samples 201021 and 201023, the use He dilution led to a substantial increase in the SAXS. Since these samples do not show a tilting effect, the added scatterers are randomly oriented or spherical in shape. Note that the use of He was accompanied by the use of larger chamber pressures and plasma powers which caused significantly higher deposition rates. The latter are similar to those of the highest used in the USSC study described above where it was also found that there was an increase in SAXS but no titling effect. Increasing the substrate temperature to 320°C caused a reduction in the SAXS for the He-diluted films; however, increasing the applied rf power by 5 W appears more effective in reducing the SAXS.

Included in Table 4 are values of the microstructure factor R, determined by IR measurements. While a trend of increasing Q with increasing R is seen for the undiluted films, the data from the He-diluted films do not support this trend, suggesting that a

one-to-one correspondence of SAXS Q-values and IR R-values does not exist. This is not unexpected since the R-values may be infuenced by isolated Si-H_2 defects not detected in the SAXS.

Table 4. Deposition conditions, SAXS Q-values, and opto-electronic properties of a-Si:H prepared with and without He dilution.

Sample	T_s (°C)	Appl. Power (W)	He Dil ?*	Chamber Pressure (mTorr)	Q_{SAXS} (nm^{-2})	depositon rate (Å/sec)	E_o PDS (meV)	R	N_d PDS (cm^{-3})
201041	50	2	No	40	7.4×10^{-6}	0.5	-	0.5	$> 1 \times 10^{17}$
201031	100	2	No	40	1.4×10^{-6}	0.6	~60	0.2	$\sim 4 \times 10^{16}$
201021	250	1	No	40	2.5×10^{-7}	1.0	~52	0.1	$\sim 1 \times 10^{16}$
201023	250	15	Yes	550	3.1×10^{-6}	8	~52	0.4	$\sim 1 \times 10^{16}$
201051	320	15	Yes	550	1.4×10^{-6}	12	54	0.5	$\sim 1 \times 10^{16}$
201052	260	20	Yes	550	2.2×10^{-6}	5	~52	0.3	$\sim 1 \times 10^{16}$

* 40% SiH_4 in He

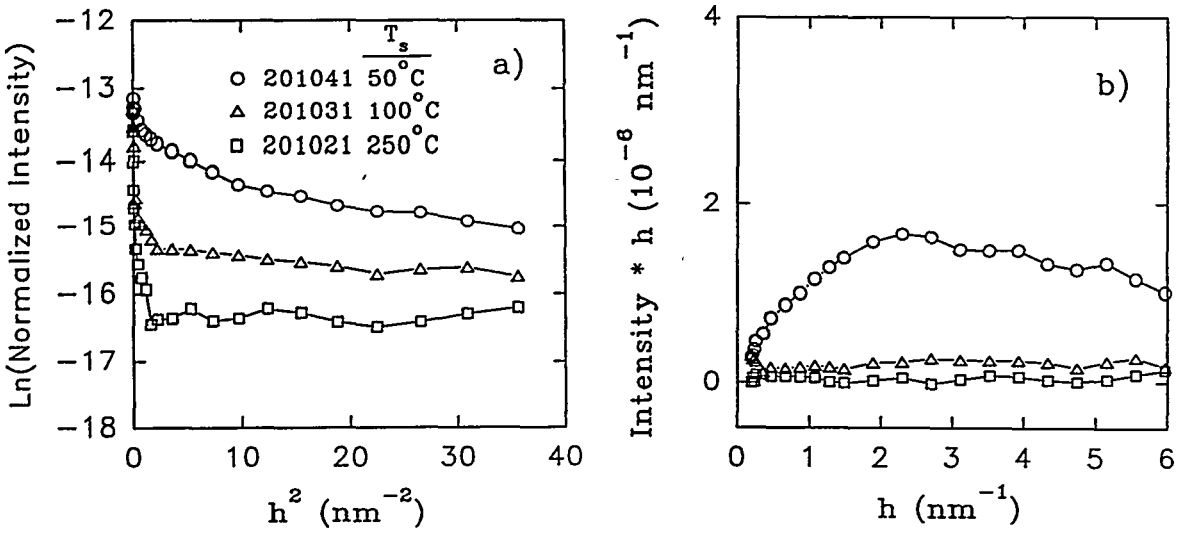

Fig. 5. SAXS versus substrate temperature for a-Si:H prepared without He dilution.
a) Guinier plots (no correction for Laue mon.); b) I x h plots.

3.4 ECR Xe dilution and other variables

Several of the ECR-deposited samples supplied by the JPL group were prepared under Xe dilution conditions. These films were all examined by EPMA for residual Xe and none was found (< 1 at. %). SAXS data from several samples are shown in Fig. 6 where clear differences can be seen. The deposition conditions and the accumulated results from all 13 ECR samples (including 6 from last year) are compiled in Tables 5 and 6, respectively. Seven deposition parameters were varied so it is difficult to establish any systematic trends. In general the photo/dark conductivities appear quite high when correlated with the Q-values compared to results from a-Si:H prepared by other standard PECVD or VHF-PECVD (see Tables 3, 4 and 6). Also, the Q-values tended to be somewhat smaller for the films prepared under Xe dilution conditions. One of these, however, was subjected to "H_2-annealing" and clearly has a larger amount of microstructure and a much-reduced photoconductivity.

An unusual feature detected in the ECR SAXS data from two samples is an opposite trend due to tilting, i.e. the SAXS intensity *increased* upon tilting the samples at ± 45 degrees. The approximate independence of the positive or negative tilt together with the increase suggests that disc-like scattering centers are present with a preferred orientation within the film plane.

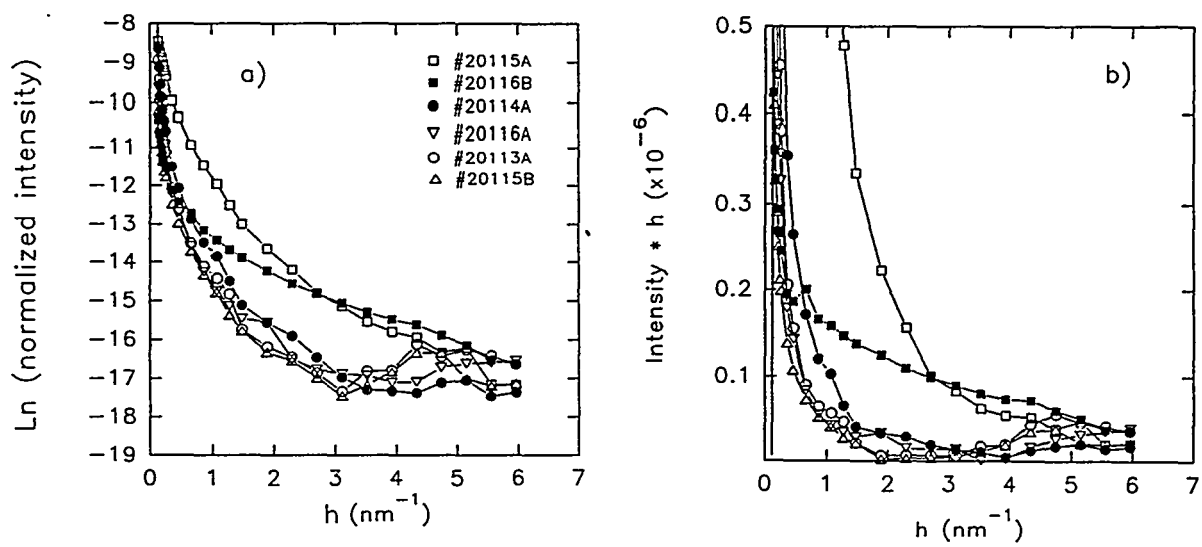

Fig. 6. SAXS from several ECR-produced a-Si:H films. a) Ln I vs h plots; b) I x h plots.

Table 5. Deposition parameters used for the ECR-produced films.

Sample	T_s (°C)	Appl. Power Incident/ Reflected (W)	Mag. Field Top Coil/Bottom Coil (Amp)	Chamber Pressure (mTorr)	SiH_4 Flow (sccm)	H_2 Flow (sccm)	Xe Flow (sccm)
10716A	275	299/31	125/30	0.6	10	30	0
10717A	275	299/82	116/116	0.6	10	30	0
10717B	275	299/87	123/45	4	15	45	0
10719	250	299/96	123/45	4	15	45	0
10722A	250	299/92	123/45	5	15	45	0
10722B	250	299/85	124/40	5	40	40	0
20113A	350	299/60	114/135	3	20	40	15
20113B	350	299/50	135/135	3	20	40	15
20114A	400	300/55	113/135	3	20	40	15
20115A	350	300/64	113/135 H_2 annealing	3	20	40	15
20115B	350	300/60	135/135	1	20	0	15
20116A	250	298/58	135/135	1	20	0	15
20116B	250	298/50	135/135	4	20	0	0

Table 6. SAXS, flotation density, and opto-electronic data for the ECR-produced films.

Sample	σ_{dark} ($[\Omega cm]^{-1}$)	σ_{photo} ($[\Omega cm]^{-1}$)	$\sigma_{photo}/\sigma_{dark}$	E_o (meV)	N_s (cm^{-3})	Q_{SAXS} (nm^{-2})	Density (g/cm^3)
10716A	3.6×10^{-11}	3.4×10^{-5}	9.4×10^{5}	63	1.1×10^{16}	2.8×10^{-6}	-
10717A	4.5×10^{-11}	2.7×10^{-6}	6.0×10^{4}	107	4.1×10^{16}	3.1×10^{-5}	-
10717B	-	-	-	-	-	6.4×10^{-6}	-
10719	1.7×10^{-12}	3.2×10^{-6}	1.9×10^{6}	52	4.0×10^{15}	5.1×10^{-6}	-
10722A	-	-	-	-	-	5.5×10^{-6}	-
10722B	-	-	-	-	-	2.3×10^{-6}	-
20113A	4.6×10^{-12}	1.0×10^{-5}	2.2×10^{6}	-	-	3.0×10^{-6}	2.25
20113B	5.2×10^{-12}	3.0×10^{-5}	5.8×10^{6}	-	-	-	2.25
20114A	5.8×10^{-12}	2.1×10^{-5}	3.6×10^{6}	-	-	3.6×10^{-6}	2.26
20115A	1.9×10^{-9}	3.9×10^{-6}	2.1×10^{3}	-	-	1.8×10^{-5}	2.19
20115B	1.3×10^{-11}	3.6×10^{-5}	2.8×10^{6}	-	-	1.8×10^{-6}	2.23
20116A	1.5×10^{-11}	1.1×10^{-5}	7.3×10^{5}	-	-	2.2×10^{-6}	2.20
20116B	2.3×10^{-12}	4.0×10^{-6}	1.7×10^{6}	-	-	5.9×10^{-6}	2.12

3.5 RMS a-Si:H

3.5.1 Variation of H-content

The effect of the hydrogen partial pressure, P_{H2}, used during RMS deposition of a-Si:H films has been examined with a set of samples from the group at the University of Illinois. All samples of the set were made at the same substrate temperature of 230°C. Systematic increases in the SAXS with increasing P_{H2} are shown in Fig. 7. Tilting studies demonstrate that most if not all of the scattering centers added with increasing P_{H2} are oriented in a way consistent with columnar-like growth. The Laue monotonic contribution extracted from the larger angle behavior increases with P_{H2} as expected for increased H alloying. Table 7 lists results available to date for this set of films. Of particular interest is the very small SAXS for the unhydrogenated material. We have reproduced this effect with our own rf sputtering system at CSM by using adequate power at lower Ar pressure.

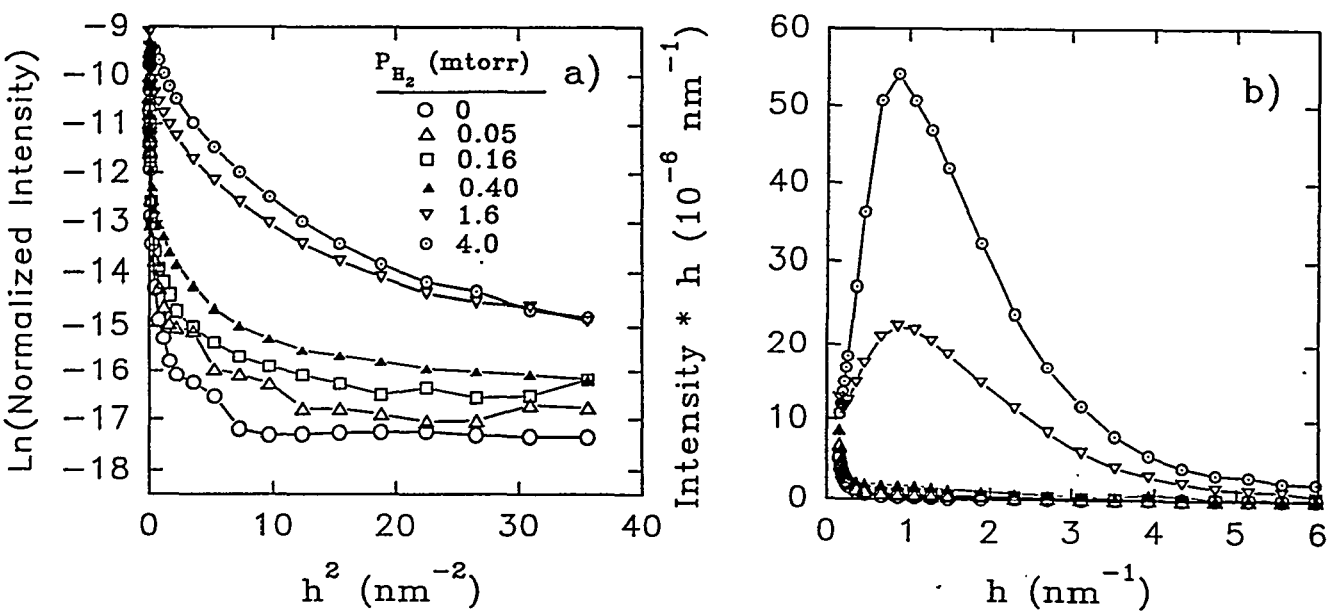

Fig. 7. SAXS from RMS a-Si:H prepared with different hydrogen partial pressures.
a) Guinier plots; b) I x h plots.

Table 7. RMS film preparation conditions, thicknesses, SAXS, and flotation results

Sample	P_{H2} (mTorr)	Anode Bias (V)	Grounded Electrode?	Film Thickness (μm)	Q_{SAXS} (nm^{-2})	Q_0/Q_{45}	Laue mono. intensity	Film Density (g/cm^3)
1778T	0	15	Yes	2.5	8.7×10^{-7}	-	3.6×10^{-8}	2.30
1791T	0	15	Yes	8	2.4×10^{-6}	-	4.2×10^{-8}	2.29
1788T	0	70	Yes	8.5	2.8×10^{-6}	3.86	5.9×10^{-8}	2.31
1788C	0	70	No	7.8	1.9×10^{-6}	-	5.7×10^{-8}	-
1779T	0.05	15	Yes	2.5	1.5×10^{-6}	-	4.5×10^{-8}	2.29
1780T	0.16	15	Yes	2.4	2.1×10^{-6}	4.67	5.3×10^{-8}	2.26
1790T	0.4	15	Yes	2.7	5.0×10^{-6}	-	6.9×10^{-8}	2.21
1793T	0.4	70	Yes	2.8	5.5×10^{-6}	-	1.7×10^{-7}	2.20
1781T	1.6	15	Yes	1.8	5.1×10^{-5}	-	2.5×10^{-7}	2.15
1782T	4.0	15	Yes	1.3	1.1×10^{-4}	3.59	-	2.09

3.5.2 Higher substrate temperatures

Another set of 6 RMS a-Si:H films from the same group was prepared to explore effects of higher substrate temperatures, T_s. All other deposition conditions were fixed while T_s was varied from 150 to 425°C. All samples were checked by x-ray diffraction for evidence of crystallinity and none was found. Figure 8 documents the changes in SAXS with increasing T_s. The largest change occurred between 150 and 300°C although a significant decrease also occurred for the relatively small T_s change from 400 to 425°C. Numerical results are listed in Table 8 together with Laue monotonic contributions. The latter scale with bonded H content as expected. These samples also exhibit tilting effects associated with columnar-like microstructure. However, the higher the T_s, the smaller the degree of tilting effect as shown by the ratios Q(0)/Q(45) included in the table.

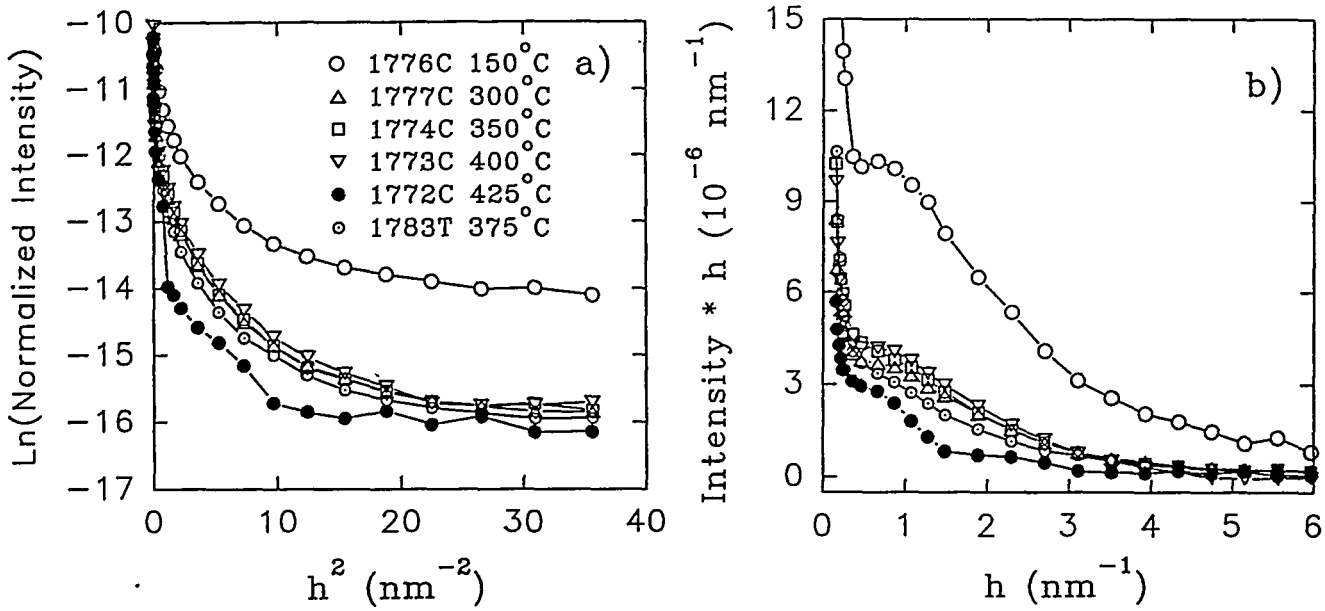

Fig. 8. SAXS from RMS a-Si:H films deposited at increasing substrate temperatures. a) Guinier plots; b) I x h plots.

Table 8. RMS a-Si:H films, substrate temperatures, SAXS, and flotation results.

Sample	P_{Ar} (mTorr)	P_{H2} (mTorr)	T_s (°C)	Film Thickness (μm)	Q_{SAXS} (nm^{-2})	Q_0/Q_{45}	Laue mono. intensity	Film Density (g/cm^3)
1776C	1.5	0.8	150	1.2	2.7×10^{-5}	-	6.2×10^{-7}	2.11
1777C	1.5	0.8	300	2.8	8.2×10^{-6}	-	9.5×10^{-8}	2.19
1774C	1.5	0.8	350	2.0	8.6×10^{-6}	-	1.1×10^{-7}	2.21
1783T	1.5	0.8	375	2.4	7.1×10^{-6}	-	8.3×10^{-8}	2.23
1773C	1.5	0.8	400	2.0	8.4×10^{-6}	2.80	1.5×10^{-7}	2.23
1772C	1.5	0.8	425	2.3	3.5×10^{-6}	1.75	8.7×10^{-8}	2.25

3.6 IACS material

Three a-Si:H films were prepared at the Indian Association for the Cultivation of Science (IACS) at different *cathode* temperatures while other deposition parameters were nominally fixed (see Table 9). The small slopes in the SAXS curves of Fig. 9 show that most of the scattering centers are relatively small and the Q-values, listed in Table 9, are at least three times larger than those typically found for device-quality, PECVD a-Si:H. The larger amount of microstructure in the IACS films is likely related to the relatively high deposition rates of 0.7 to 1.0 nm/s. A fourth film prepared under more H_2 dilution (50 sccm vs 20 sccm) showed a significant decrease in the SAXS, consistent with a reduced deposition rate for this film.

Upon tilting the films at 45 degrees, the SAXS decreased consistent with columnar-like growth. The size distribution of the scattering centers in these films is dominated by about 80 to 90 vol.% of the voids having minor-axis diameters of only 0.8 nm.

Table 9. Deposition conditions and SAXS results for IACS a-Si:H films.

Sample	SiH_4 flow (sccm)	H_2 flow (sccm)	$T_{cathode}$ (°C)	deposition rate (Å/s)	Q_{SAXS} (nm^{-2})	Q_0/Q_{45}	Film density (g/cm^3)
CH 29	20	20	140	7.7	8.1×10^{-6}	1.36	2.08
CH 25	20	20	200	9.8	3.1×10^{-6}	1.48	2.16
CH 42	20	20	235	10	4.1×10^{-6}	-	2.16
CH 33	20	50	200	3.2	1.4×10^{-6}	1.74	2.20

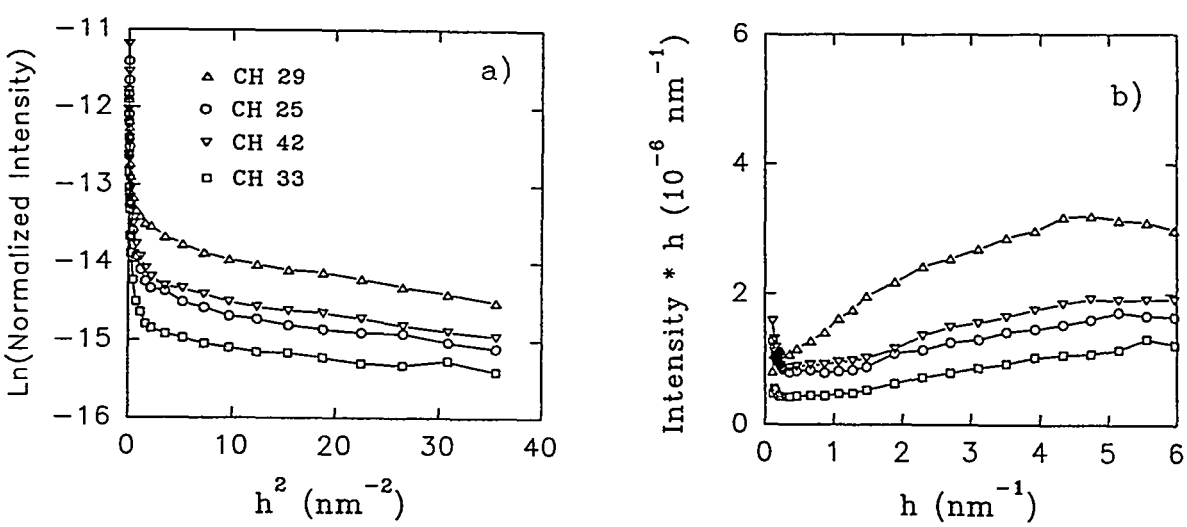

Fig. 9. SAXS data for ICAS a-Si:H films prepared while heating the cathode of a PECVD system. a) Guinier plots; b) I x h plots.

4. ALLOYS

4.1 a-SiGe:H microstructure transition

A correlation of SAXS, film flotation density, electron microprobe and opto-electronic measurements on co-deposited a-$Si_{1-x}Ge_x$:H films in a series covering the range $0 \leq x \leq 0.37$ provides strong evidence that the appearance of oriented microstructure above a well defined value of x is responsible for the degraded opto-electronic behavior [2].

Samples were prepared by the Stuttgart University group using a DC glow-discharge system in a triode configuration [18]. Films with thicknesses of 2.5-2.7 μm were co-deposited on 10-μm Al foil for SAXS, electron microprobe and film flotation density measurements, on Corning 7059 glass for opto-electronic measurements, and on c-Si wafers for IR measurements. Throughout the series of depositions, germane and silane flows were altered to vary x while all other parameters remained fixed at the following values: substrate temperature=200°C; chamber pressure=0.34 mbar; total germane+silane gas flow=30 sccm; hydrogen gas flow=20 sccm; power density=50 mW/cm^2.

Figure 10 displays the SAXS data in the form of the product of the normalized scattering intensity and h versus h plots. Contributions due to Laue monotonic scattering were clearly present and subtracted.

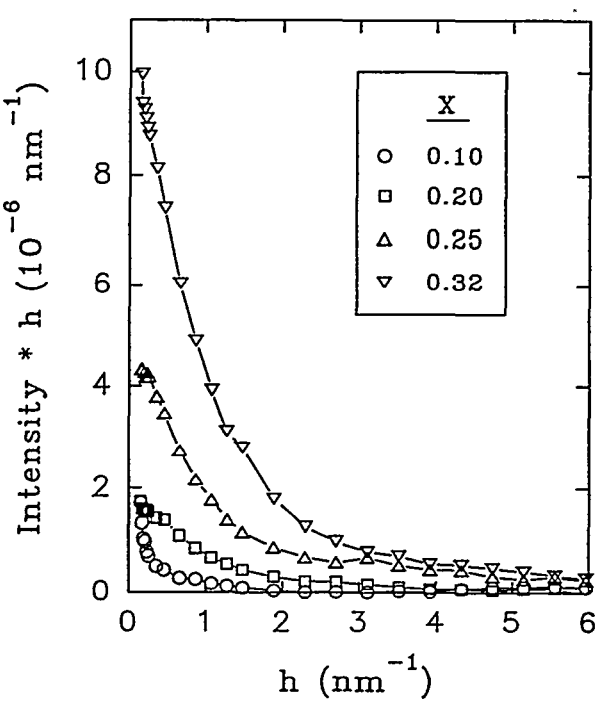

Fig. 10. SAXS data for a-$Si_{1-x}Ge_x$:H films.

The Q-values rise significantly above x=0.2 as is shown in Fig. 11a. Enhanced density contrasts due to the increased electron density of the bulk matrix with the addition of Ge cannot account for such a rise. This increase in Q as well as the accompanied increase in defect density, N_d, detected by sub-bandgap absorption, also shown in Fig. 11a, suggest that a more defective, heterogeneous microstrucure forms above x=0.2.

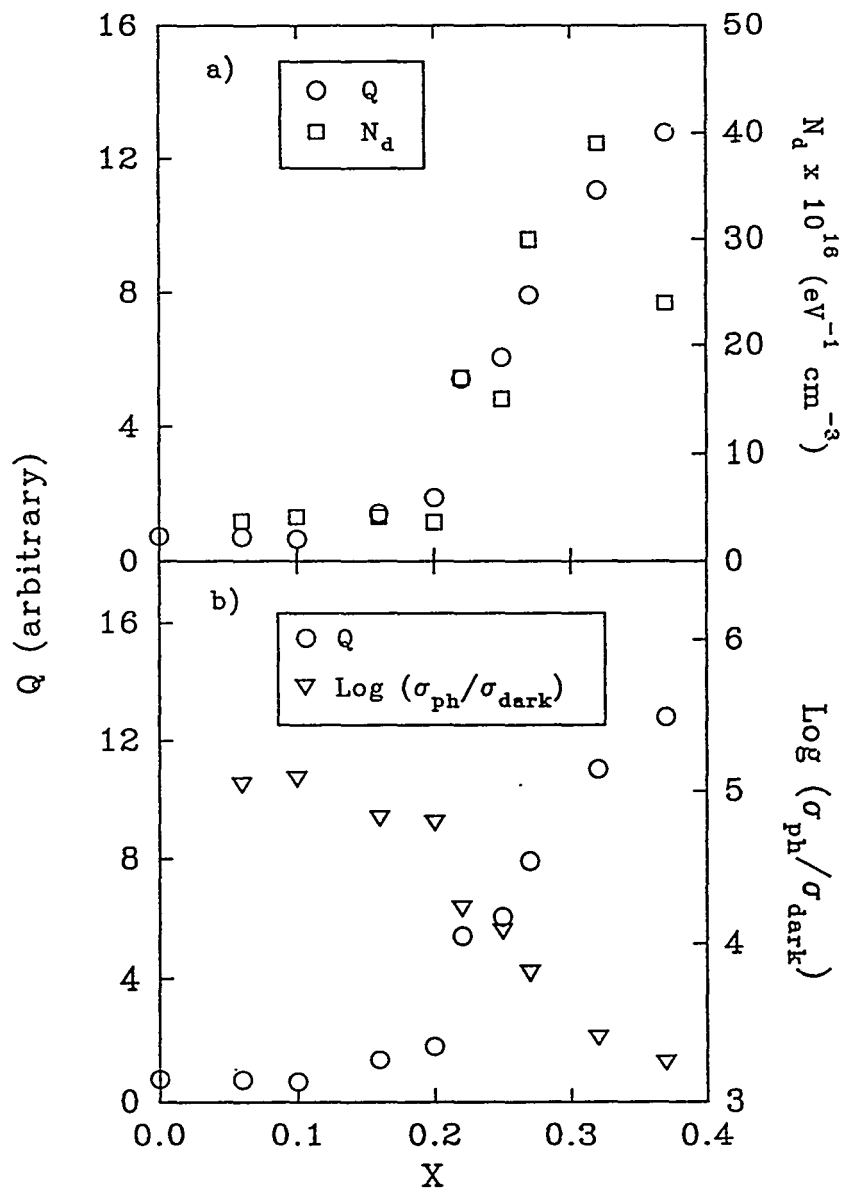

Fig. 11. Variations in a)Q and N_d and b) Q and Log($\sigma_{ph}/\sigma_{dark}$) with x.

The ratio of photo-to-dark conductivity, $\sigma_{ph}/\sigma_{dark}$, exhibits a sharp decrease as x increases above 0.2 correlating with the increase in Q as is shown in Fig 11b. Again, this is evidence that the source of the opto-electronic degradation is the additional heterogeniety.

Fitting the SAXS curves to a superposition of theoretical curves based on up to 5 sizes of spherical scattering centers, it was found that increases in the volume fraction of scattering centers with 3 to 4 nm diameters can account for the observed increases in Q. However, as shown in Fig. 12, tilting effects were clearly evident in the SAXS for samples with x above x=0.2 and this requires the presence of non-spherical, oriented scattering centers, consistent with columnar-like growth. In this case, the above diameters represent the smaller cross-sectional diameter of elongated scattering centers oriented with the long axis parallel to the film growth direction.

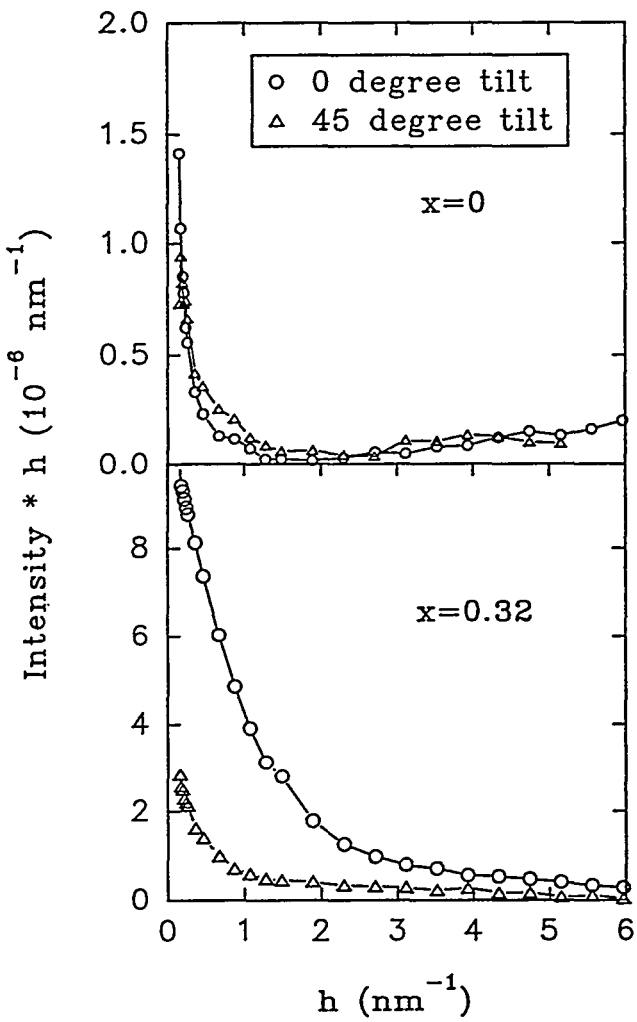

Fig. 12. Effect of tilting on the SAXS intensity for two values of Ge content (x).

Density deficits can be estimated from the precision flotation density results shown in Fig. 13. The deficits are given by the difference between the experimental densities and those of crystalline material indicated by the solid and dashed lines, based on Vegard's law and EXAFS data, respectively [2]. Density deficits gradually increase from about 1 to 4% with increasing Ge content based on comparison with the Vegard's law curve and do not show evidence of a sharp change above x=0.2. This at first appears to contradict the SAXS behavior, however, oriented, elongated scattering centers can cause significant enhancements in the SAXS relative to a randomly oriented distribution with the same volume fraction.

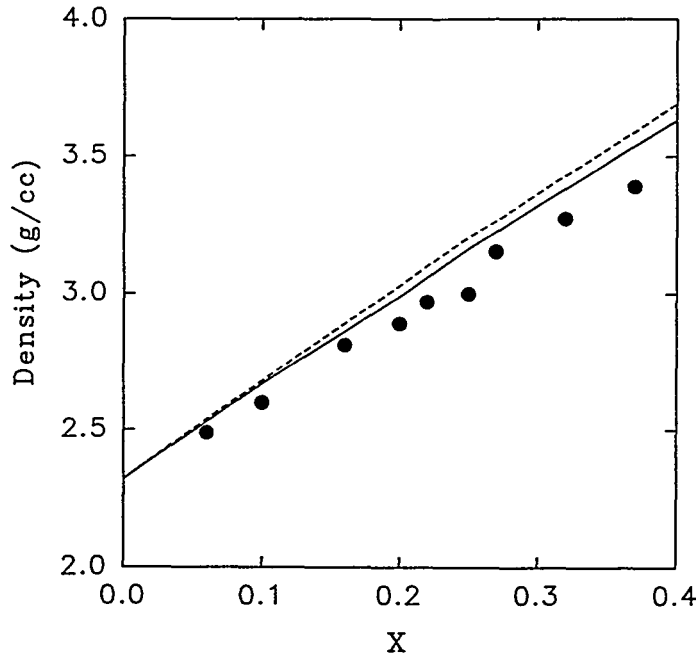

Fig. 13. Flotation density results compared with crystalline densities.

The SAXS results are therefore interpreted to demonstrate a transition in the microstructure from a relatively homogeneous, dense state for x<0.2 to an increasingly heterogeneous, lower density one for x>0.2. The transition involves the formation of a columnar-like structure and is consistent with earlier TEM studies of a-SiGe:H alloys with $x \simeq 0.5$ [19]. It seems quite likely that the SAXS originates from low density regions between the columns and these are likely to be microvoids based on models of the origin of columnar microstructure [20] and our observation of density deficits. However, the presence of hydrogen-rich "tissue" [19] could produce similar scattering due to weak x-ray scattering by H atoms.

The appearance of columnar-like microstructure above x=0.2 is suggested to be due to a reduced average surface mobility of the depositing radicals for higher fractions of

germane in the plasma. The reduced mobility limits island coalescence and self-shadowing leads to column formation [20]. The origin of the well-defined value of x=0.2 above which the surface mobility becomes too small is not known, but it should be possible to increase this value by increasing the substrate temperature, reducing the deposition rate (lower power) or by modifying the hydrogen dilution. Based on the strong correlation observed here, improved opto-electronic properties should accompany the removal of this heterogeneous type of microstructure as long as alteration of the deposition conditions does not reduce the hydrogen content to a point where isolated defects in the bulk begin to offset any improvements.

4.2 Comparison of PECVD films from several groups

We now have analyzed many a-SiGe:H films from several groups in addition to those described above from Stuttgart University, including sets from NREL, Solarex, USSC, Princeton University, and IACS. Table 10 presents the SAXS and other results from this extensive set of alloy films. Important aspects of these results are discussed below.

4.2.1 Laue monotonic effect

A random binary alloy, $A_{1-x}B_x$, should produce a background x-ray scattering effect, the Laue monotonic contribution, that is proportional to $(f_A - f_B)^2(1-x)x$, where f_i is the atomic form factor [21]. Since the latter decreases only slightly from $f_i=Z_i$, the number of electrons on the atom, at zero scattering angle up to the largest angle probed in our SAXS measurements, an essentially angle-independent contribution is expected. Evidence for this effect is readily seen from the SAXS of the SiGe alloys: at the higher angles the scattering intensity approaches a constant value that is correlated with the Ge content. Using a procedure outlined in section 6.1, this background intensity, I_{LM}, is extracted for each of the samples. Figure 14 displays values of I_{LM} for all of the a-SiGe:H samples investigated to date as well as several a-Si:H and a-Ge:H samples. The solid line is a least-square fit to a quadratic in x consistent with the theoretical expression cited above.

The scatter in the data is due in part to uncertainties in extraction of this relatively small background effect. However, a refinement of the theory to include the effect of H alloying shows that some of the scatter could be due to H content variations. Assuming a random ternary alloy of $Si_{1-x-y}Ge_xH_y$, one can show the Laue monotonic intensity is given by:

$$I_{LM} = C[(Z_{Ge}-Z_{Si})^2(1-x-y)x + (Z_H-Z_{Si})^2(1-x-y)y + (Z_{Ge}-Z_H)^2xy],$$

Table 10. SAXS and flotation density results for a-$Si_{1-x}Ge_x$:H alloys from several groups.

Sample	Ge content (x)	Q_{SAXS} (nm^{-2})	Laue monotonic intensity	Q_0/Q_{45}	Film Density (g/cm^3)	Density Deficiency (%)
IACS GH-14	0.15	5.8×10^{-6}	3.6×10^{-7}	1.7	2.68	5.3
IACS GH-8	0.22	1.5×10^{-6}	4.3×10^{-7}	4.2	2.89	5.6
IACS GH-9A	0.26	5.0×10^{-6}	4.6×10^{-7}	1.2	2.98	6.6
IACS GH-21	0.34	3.1×10^{-6}	4.4×10^{-7}	4.4	3.26	5.2
IACS GH-23	0.37	7.3×10^{-6}	4.4×10^{-7}	2.6	3.32	6.2
IACS GH-19A	0.47	6.1×10^{-6}	4.5×10^{-7}	-	3.56	7.3
IACS GH-26	0.54	2.1×10^{-5}	4.9×10^{-7}	-	3.75	7.4
IACS GH-43	0.57	1.5×10^{-5}	4.8×10^{-7}	2.3	3.94	4.8
IACS GH-30	0.68	2.4×10^{-5}	3.3×10^{-7}	4.1	-	-
IACS GH-31	0.72	4.0×10^{-5}	3.0×10^{-7}	-	-	-
USSC 5525	0.09	1.3×10^{-6}	2.6×10^{-7}	0.99	2.54	3.4
USSC 5526	0.09	4.2×10^{-7}	2.8×10^{-7}	-	2.61	0.7
USSC 4838	0.19	1.1×10^{-6}	3.2×10^{-7}	0.74	2.98	-0.7
USSC 4835	0.31	2.4×10^{-6}	5.2×10^{-7}	1.3	3.26	2.7
USSC 4837	0.41	6.3×10^{-6}	4.4×10^{-7}	2.7	3.50	4.4
USSC 5445	0.44	9.2×10^{-6}	3.7×10^{-7}	5.3	3.60	4.0
Stuttgart H204281	0.06	7.4×10^{-7}	2.5×10^{-7}	-	2.49	1.6
Stuttgart H205041	0.10	6.8×10^{-7}	2.7×10^{-7}	1.2	2.60	2.6
Stuttgart H205061	0.16	1.5×10^{-6}	4.0×10^{-7}	-	2.81	1.8
Stuttgart H205111	0.20	1.9×10^{-6}	4.0×10^{-7}	2.6	2.89	3.3
Stuttgart H208191	0.22	5.4×10^{-6}	3.8×10^{-7}	-	2.97	2.9
Stuttgart H208171	0.25	6.0×10^{-6}	4.0×10^{-7}	2.6	3.00	5.1
Stuttgart H208211	0.27	7.9×10^{-6}	4.8×10^{-7}	-	3.15	2.2
Stuttgart H205191	0.32	1.1×10^{-5}	4.8×10^{-7}	4.6	3.27	3.3
Stuttgart H205211	0.37	1.3×10^{-5}	4.5×10^{-7}	-	3.39	4.2
Solarex 00164-1	0.40	7.8×10^{-6}	4.7×10^{-7}	-	3.39	6.6
Solarex 00163-2	0.42	1.4×10^{-5}	4.9×10^{-7}	-	3.39	8.1
Princeton S4	0.15	8.7×10^{-6}	-	0.77	2.69	5.0
Princeton M281	0.23	6.9×10^{-6}	-	1.2	2.97	3.9
Princeton S2	0.24	1.2×10^{-5}	-	1.0	2.92	6.7
Princeton S3	0.32	8.3×10^{-6}	-	1.1	-	-
NREL 922	0.72	4.2×10^{-5}	3.6×10^{-7}	-	-	-

where C is a constant related to the conversion of the experimental intensity into absolute scattering units (electron units). The relative strength of the three terms is seen after substitution of the atomic numbers:

$$I_{LM}=C[324(1-x-y)x + 169(1-x-y)y + 961xy].$$

Calculations based on this equation are shown in Fig. 15 where the effect of various constant H contents are considered (i.e., x is varied for constant, selected y). Also shown are calculations for a-SiC:H alloys (same selected y values) to demonstrate the much smaller size of the Laue monotonic effect compared to the a-SiGe:H alloys. Note the relatively strong effect of slight variations in H content supporting the above suggestion that some of the scatter in Fig. 14 is due to this. Also note the effect of H on the asymmetry in the parabolic shape, evidence of which is also seen in the fit to the experimental data in Fig. 14. Further confirmation that we are observing the effect of random alloy scattering is the relative change in I_{LM} between x=0 and x near 0.5 where the maximum occurs, i.e. compare the relative increase in values at x=0 and x near 0.5 in the theoretical and experimental curves. This is further illustrated by the dashed curve in Fig. 14 which was obtained from the above equation by using y=0.10 for x=0 (typical H content in a-Si:H) and allowing it to drop linearly to y=0.03 for a-Ge:H (typical value for the a-Ge:H films).

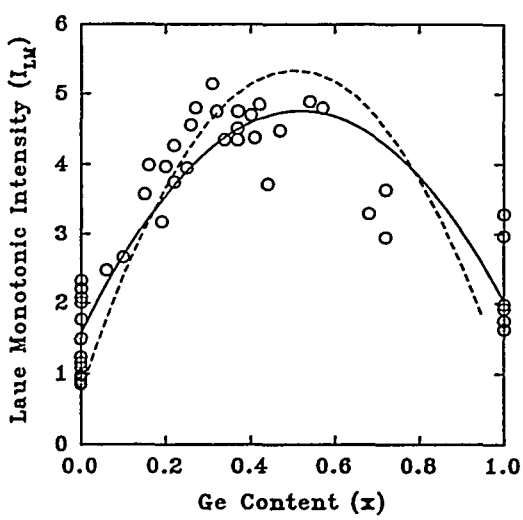

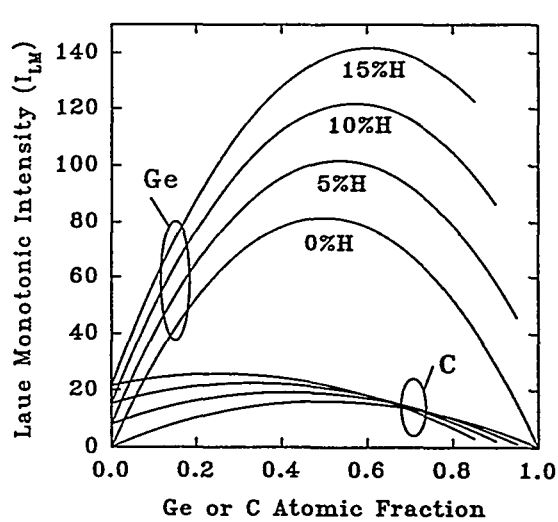

Fig. 14. (left)Experimentally determined background signals from a-SiGe:H alloys.

Fig. 15. (right) Theoretical Laue monotonic scattering contributions expected for a-SiGe:H and a-SiC:H alloys of various H contents.

We plan to generate a set of unhydrogentated SiGe alloys using the sputtering system at CSM to eliminate the effect of H and thereby obtain a better quantitative value for C, the constant in the above equation. This will allow sound theoretically-based corrections for the Laue monotonic contributions to the SAXS data and more accurate determination of the nature of the microstrucural features causing the angle-dependent SAXS. It may also allow the SAXS data to be used to provide independent information on the degree of alloy randomness. For example, clustering of Ge or H should reduce the size of I_{LM} and result in a corresponding increase in the SAXS provided the clusters are larger than the few atom sizes associated with those of random alloying.

4.2.2 Integrated SAXS and tilting effects

The Q-values listed in Table 10 and other tables in this report are all corrected for the Laue monotonic contribution and represent the integrated SAXS due to the larger scale microstructural features. Trends in Q with x (where x is now the fractional Ge content as represented by a-$Si_{1-x}Ge_x$:H) are shown in Fig. 16 for all samples examined to date. The expected increase in Q due simply to the larger electron density contrast upon adding Ge, assuming only voids produce the SAXS, is shown by the dashed curve. For alloys with $x \leq 0.2$, all but two of the films have $Q \leq 2$ with 0.4 being the lowest value. In the range $0.2<x<0.4$, the Q values are notably higher with an average near Q=7. The average increases for x>0.4 but drops noticeably at x=1 for several of the Harvard a-Ge:H samples.

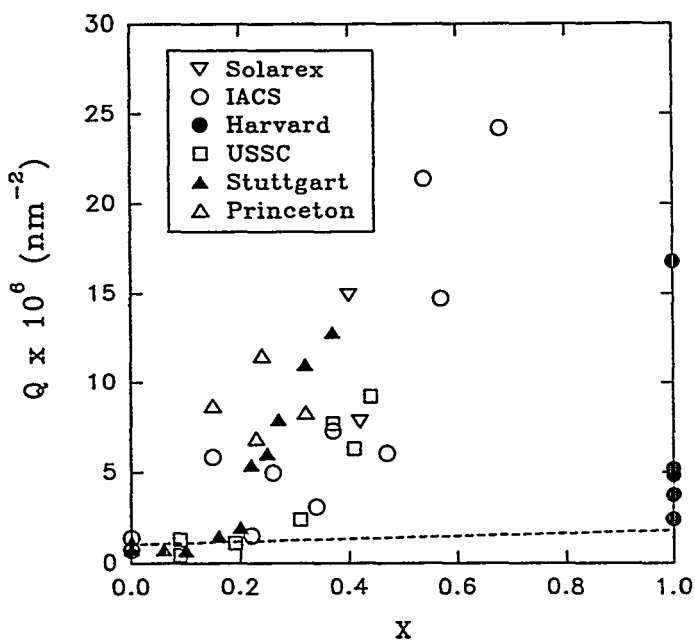

Fig. 16. SAXS Q-values versus Ge content for a-SiGe:H alloys from several groups.

Another important trend with x is an increase in the amount of elongated, preferential oriented scattering centers. This can be seen in Fig. 17 where the ratio of the non-tilted to 45°-tilted integrated SAXS, Q_0/Q_{45}, is plotted versus x. Below x=0.2 the ratio for most films is near unity, indicating little change upon tilting and a relatively homogeneous microstructure (spherical scatterers or randomly oriented non-spheres). For 0.2<x<0.4 most of the films show ratios above 2, but a few remain low. Above x=0.4 all of the samples have a ratio greater than 2 including the a-Ge:H films. Thus the larger Ge fractions lead to more oriented microstructure characteristic of columnar-like growth. A noteworthy feature of the films made at Princeton University using GeF_4 rather than germane as the Ge source, is the lack of a strong tilting effect for any of the samples.

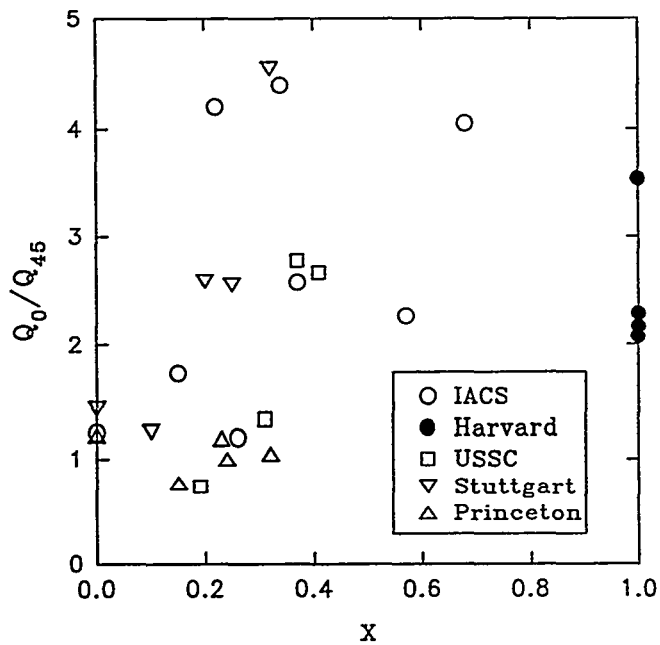

Fig. 17. Tilting effect ratio versus Ge content for a-SiGe:H films from several groups.

The third general trend that we find in the a-SiGe:H alloys upon analysis of the size distributions is an increase in the fraction of scatterers with diameters between 3 and 4 nm as is shown in Fig. 18. These diameters are determined from the SAXS data at zero tilt angle and for the samples showing the oriented, elongated scattering centers, such diameters represent those of the minor axis. As will be described later in section 6.2, an extention of our modeling to determine the approximate size of the long axis based on the treatment of the tilt data has been developed.

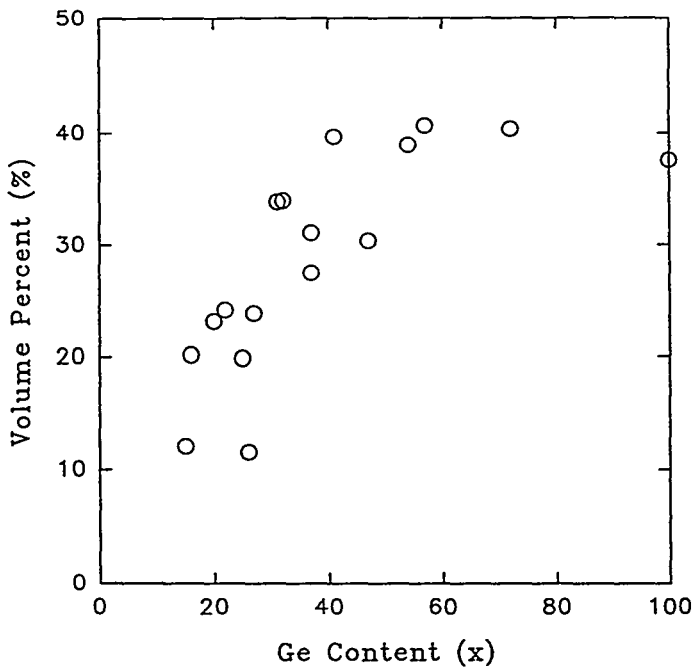

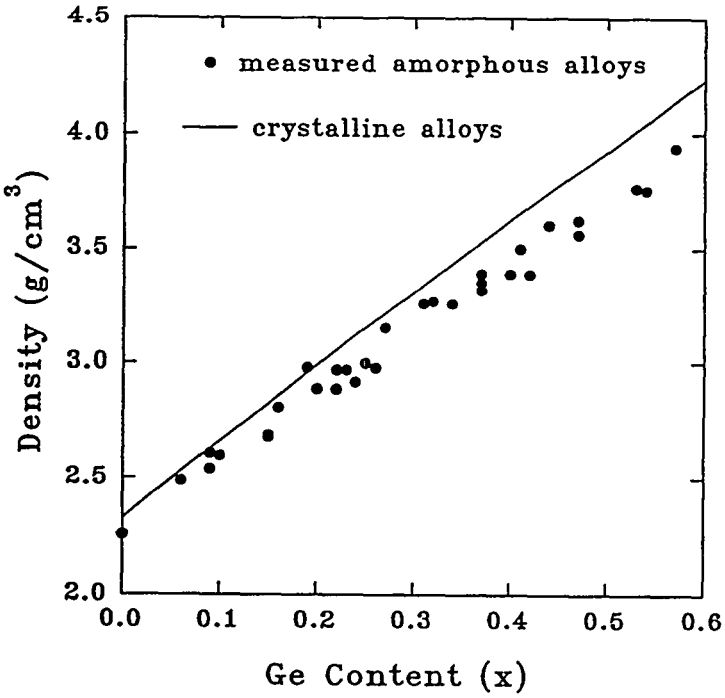

Fig. 18. (left) Fraction of scattering centers that have a minor-axis diameter between 3 and 4 nm based on size distribution fitting of SAXS data from non-tilted a-SiGe:H alloys.

Fig. 19. (right) Flotation density results (circles) compared to crystalline densities based on Vegard's law (line).

4.2.3 Flotation densities

Figure 19 shows the measured densities as a function of Ge content for most of the a-SiGe:H films received to date with $x<0.6$, corresponding to densities less than 4.05 g/cm^3, the density-limit of our flotation fluid. The solid curve in the figure represents crystalline alloy densities based on Vegard's law. Density deficits tend to increase from about 1% to 6% as x increases to about 0.6. In general these values support the interpretation of the origin of the increased SAXS as due to voids or at least significant amounts of low-density H-rich "tissue" [19], probably situated between the columns that are produced for the higher Ge-content films. This suggestion is based on the dominance of 3 to 4 nm sizes determined by SAXS compared to typical column diameters of 10 to 50 nm [19]. TEM analyses indicate the regions between the columns to be of lower density [19].

4.3 RMS a-SiC:H

A set of five a-SiC:H alloys with C contents less than 45 at.% was provided by the Illinois group. These were grown by RMS in UHV sytem using methane as the source of carbon. The SAXS data are shown in Fig. 20 after correction for the Laue monotonic background effect. The Q-values and opto-electronic data are listed in Table 11. Also included in the table are results of tilting measurements (Q_0/Q_{45}) which clearly show columnar-like microstructure in contrast with earlier results from PECVD a-SiC:H [7].

As noted in Fig. 15 earlier, alloying with C should cause an increase in the Laue monotonic contribution and as listed in the table, the experimental values indeed increase with the C fraction. The values are much larger than expected, however, so that additional atomic scale fluctuations must be present.

Results from this set of samples were analyzed on the basis of a model that considered a mixture of diamond-like and graphitic-like C incorporation in order to understand the SAXS and flotation density data [6]. The SAXS data reported there were obtained before we discovered the design flaw. Remeasurement of all the samples yields the new Q-values listed in Table 11. The qualitative conclusion reached on the basis of the flawed data remains valid: the microstructure of RMS-produced a-SiC:H is different from that of PECVD a-SiC:H in that an oriented, columnar-like growth occurs in the RMS material.

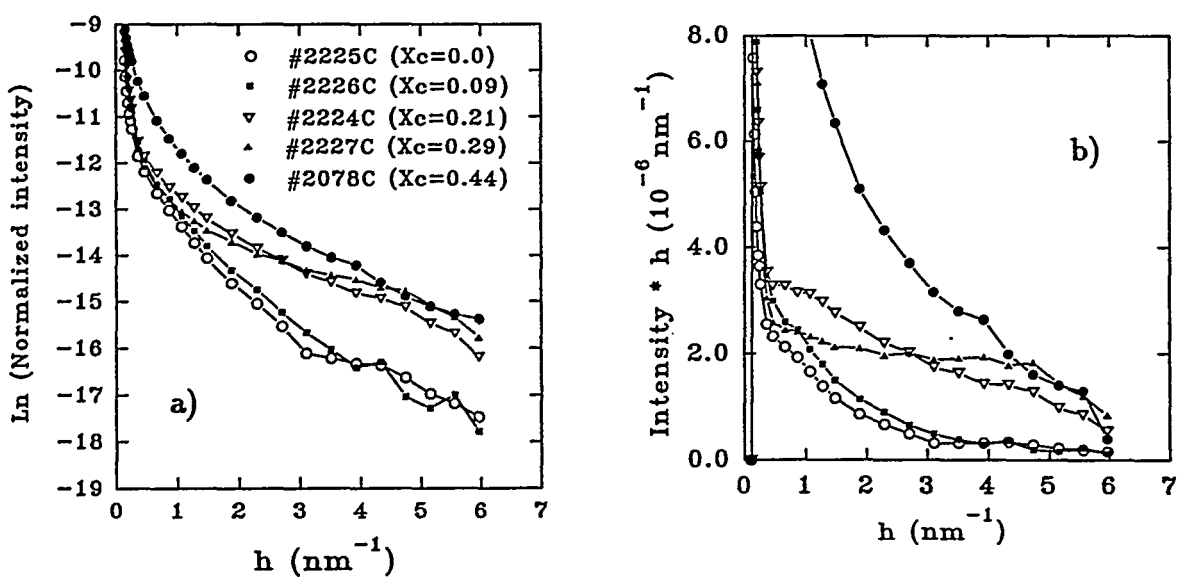

Fig. 20. SAXS from a-SiC:H alloys prepared by RMS. A constant background has been subtracted from each of the data sets. a) LnI vs h plots; b) I x h plots.

Table 11. SAXS data for RMS a-SiC:H films.

Sample	C content (x)	Film density (g/cm^3)	Q_{SAXS} (nm^{-2})	Laue monotonic intensity	Q_o/Q_{45}
2225	0	2.22	4.6×10^{-6}	1.4×10^{-7}	1.56
2226	0.09	2.17	5.9×10^{-6}	2.9×10^{-7}	-
2224	0.21	2.08	1.2×10^{-5}	6.6×10^{-7}	1.33
2227	0.29	2.10	1.2×10^{-5}	7.2×10^{-7}	1.39
2078	0.44	1.91	2.6×10^{-5}	1.2×10^{-6}	1.57

5. STUDIES of a-Ge:H

5.1 Electrode spacing study

We have examined three a-Ge:H films produced in a PECVD system at Harvard University using three different electrode separations (1.2, 2.0, and 3.2 cm). Films were deposited on both Al-foil and c-Si. In an earlier study the Harvard group demonstrated improvements in the opto-electronic properties with decreasing electrode spacing [22]. Larger photo/dark conductivity ratios, $\eta\mu\tau$ products, sharper Urbach edges and lower amounts of sub-bandgap absorption were found for the films made at the smaller spacings (see Table 12). In addition, the better device-quality films were more homogeneous as determined by TEM in contrast to the films made at 3.2 cm spacing which showed "island/tissue", columnar-type microstructure [22].

Table 12. Deposition conditions, opto-electronic data, and SAXS results for a-Ge:H films

Sample	Elect. Spacing (cm)	Appl. Power (W)	E_a (eV)	σ_o [$(\Omega cm)^{-1}$]	$\eta\mu\tau$ (cm^2V^{-1})	σ_{ph}/σ_d	E_o PDS (meV)	$\alpha_{0.7}$ PDS (cm^{-1})	E_{04} (eV)	$\alpha_{0.7} \times \eta\mu\tau$ (cmV^{-1})	Q_{SAXS} (arb.)	C_H from IR (at.%)
Harvard 257	3.2	10	0.54	8.2×10^2	2.1×10^{-9}	4.5×10^{-4}	61	65	1.16	1.4×10^{-7}	43.3	3.6
Harvard 258	2.0	10	0.56	3.6×10^4	6.0×10^{-8}	1.0×10^{-2}	54	34	1.17	2.0×10^{-6}	3.8	3.8
Harvard 259	1.2	10	0.58	9.3×10^4	1.4×10^{-7}	3.1×10^{-2}	49	18.5	1.19	2.6×10^{-6}	2.4	3.1
Harvard 340	1.4	12	0.49	2.6×10^4	4.8×10^{-8}	5.8×10^{-3}	50	13.4	1.18	6.4×10^{-7}	5.2	4.4
Harvard 338	1.4	30	0.62	6.6×10^4	3.2×10^{-7}	1.2×10^{-1}	47	10.3	1.24	3.3×10^{-6}	4.9	5.7
Harvard 342	1.4	48	0.59	1.5×10^4	6.5×10^{-8}	9.7×10^{-2}	65	66	1.20	4.3×10^{-6}	71.8	7.7

Figure 21 displays the SAXS data for the films deposited on the Al-foil substrates. The Laue monotonic background is evident, particularly for the two films grown at the smaller electrode spacings. The systematic decrease in SAXS with decreasing electrode spacing is consistent with the earlier TEM study. A particularly large decrease occurs for the change from 3.2 to 2.0 cm.

Each of the films was also measured at a 45° tilt angle and in each case the intensities decreased at smaller h values compared to the untilted cases. These decreases were larger for the larger electrode spacing samples and are again consistent with the presence of elongated, low density regions which are preferentially oriented with their major axes perpendicular to the film surface, again implying columnar-like microstructure. It is important to note that this type of microstructure is detected by SAXS in films deposited at the smallest spacing of 1.2 cm whose TEM micrographs are featureless. Calculations of size distributions show that the minor axis diameters of these elongated voids are primarily 2 to 4 nm.

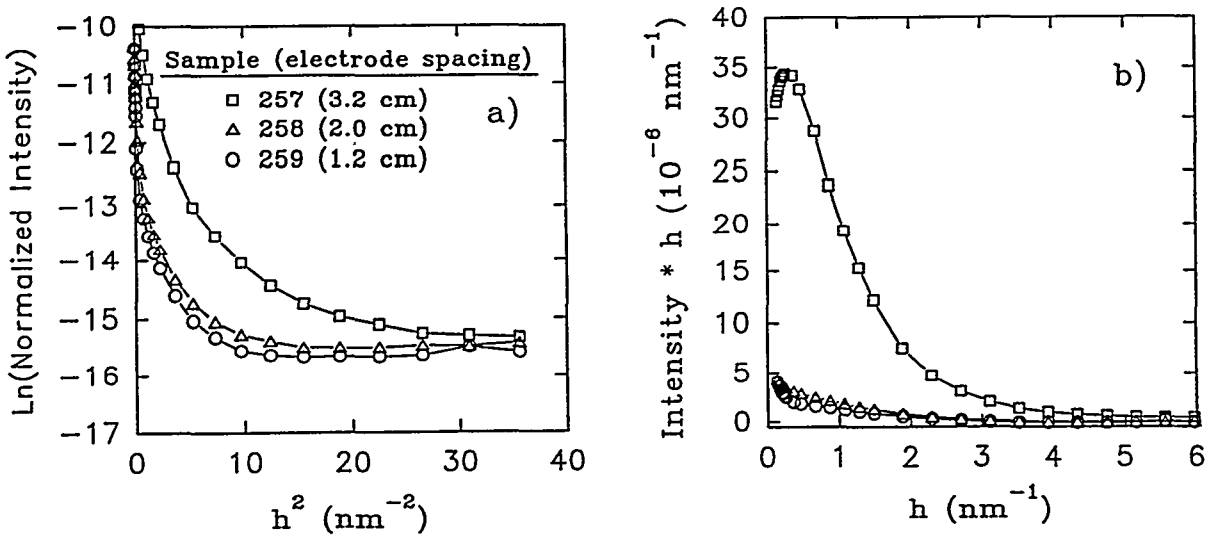

Fig. 21. SAXS data from a-Ge:H films prepared at different electrode spacings.
a) Guinier plots; b) I x h plots.

Figure 22 compares SAXS data for films deposited on Al and c-Si substrates at electrode spacings of 1.2 and 3.2 cm. The data differ only slightly in that somewhat larger intensities are obtained for h< 3 nm^{-1} for the films on c-Si. We interpret this as due to the flatness of the c-Si compared to the Al foil ($\sim 1\mu m$ roughness) so that a more highly oriented texture of the columnar-like microstructure is possible on the c-Si, leading to enhanced SAXS.

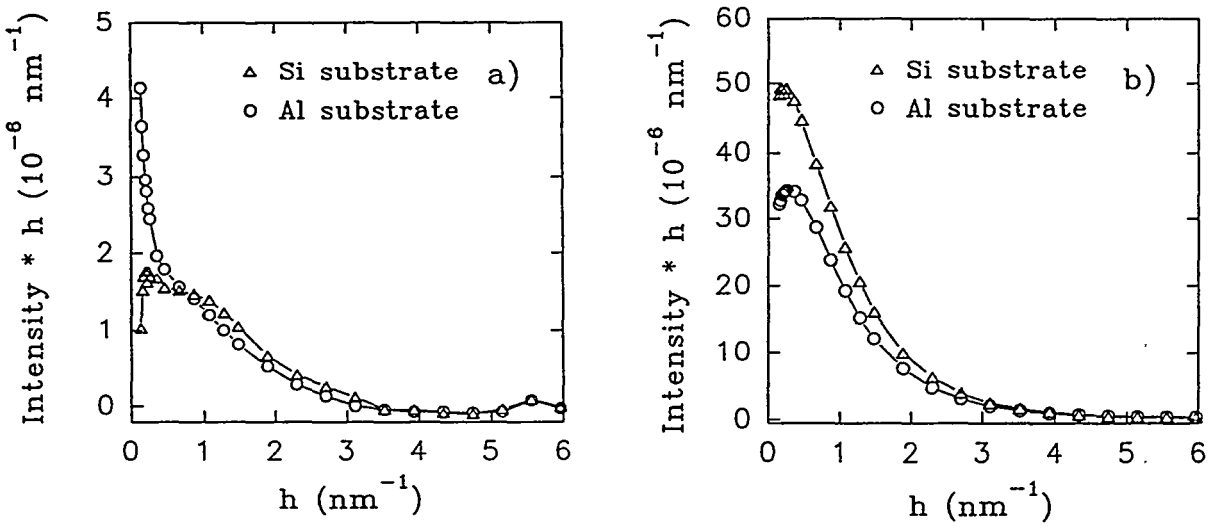

Fig. 22. I x h plots of SAXS data from a-Ge:H films prepared simultaneously on Al-foil and c-Si substrates at a) 1.2 cm and b) 3.2 cm electrode spacings.

5.2 Plasma power study

Another series of a-Ge:H films was prepared in the Harvard PECVD reactor in which three different applied rf powers were used while all other deposition parameters were nominally fixed. Prior work by the Harvard group [23] established that 30 W applied power yielded films with optimum opto-electronic properties. SAXS Guinier plots for films deposited at 12, 30 and 48 W are shown in Fig. 23a. At large h^2 the intensities become angle-independent and level off at higher intensities as the power increases. This is consistent with the reported increase in H content and the effect on the Laue monotonic scattering predicted in Fig. 15. Correction for this background then yeilds the intensity x h plots in Fig. 23b where one can see that the data from the 12 W and 30 W films are nearly identical while those from the 48 W film are much larger. In fact, the well defined "shoulder" in the Guinier plot is probably related to interference effects from closely spaced scattering centers. A model based on closely spaced spheres [8] allows an estimation of the separation of ≤ 10 nm.

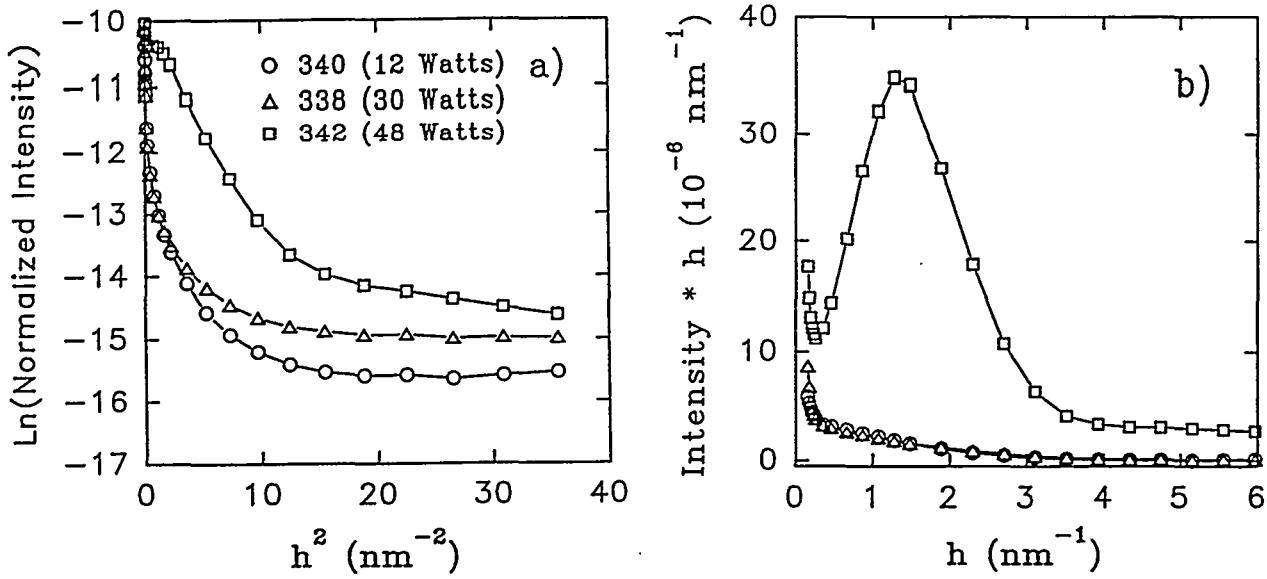

Fig. 23. SAXS data from a-Ge:H films prepared with different rf plasma powers.
a) Guinier plots; b) I x h plots.

As in the case of the electrode spacing film series, the SAXS for all of the power series depends on the tilt angle with the strongest scatterer showing the strongest tilting effect. Here also the columnar-like microstructure implied by the SAXS was not detected in TEM micrographs of 50 nm-thick films produced on Al foil at powers below 30 W [23]. There is some suggestion in TEM micrographs and clear evidence from IR data that low density regions do exist in the 48 W films [24].

Comparing the opto-electronic properties with the SAXS results (see Table 12), there are improvements as the power is increased from 12 to 30 W while essentially no change occurs in the SAXS (except for the increase in Laue monotonic scattering). Thus these improvements may be related to the increase in H content within the amorphous matrix and an associated decrease in dangling bond density rather than any change in the larger-scale microstructure. On the other hand, the obvious deterioration in the opto-electronic properties for the 48 W power is very likely associated with the increased microstructure as detected by SAXS since the H content in the matrix is even larger for this film.

For both the electrode spacing and applied power studies, we are also correlating the changes in microstructure detected by SAXS with measurements of the ion bombardment energies and the plasma chemisty made at Harvard [25].

6. DATA ANALYSIS AND MODELING

6.1 Modified analysis procedures

As mentioned previously, the repair of a design flaw in the SAXS system has led to the observation of an angle-independent contribution to many of the SAXS scans. This is attributed to the so-called "Laue monotonic" scattering and the theory behind this effect is known [21]. As documented above in the case of the many SiGe alloys, the experimental observation is clear and the quadratic dependence is consistent with theory. The extraction of this angle-independent contribution is determined in a systematic way for each set of data. Following the procedure used by others [9], a plot of the product of intensity and h^3 versus h^3 typically yields a straight line for the largest h values and the slope, obtained by least-square fitting, represents the Laue monotonic contribution. Samples containing large fractions of very small voids sometimes prevent determination of this contribution. In these cases there is little error in the void fractions or Q-values since the Laue monotonic contribution is a relatively small effect in general.

Another feature in the SAXS that is sometimes observed for the weakly scattering samples is a slight *increase* in scattered intensity with increasing angle. Again, this was detected after repair of the design flaw. Examination of the literature suggests that incoherent Compton scattering could be the origin of this effect. We have also considered the contribution of thermal-diffuse scattering based on available theory. Both are quite weak and the estimated magnitudes are consistent with the observations. Figure 24 shows the theoretical results placed on a scale appropriate to our measured intensities for both Al and Si. The increase with h is typical of what we sometimes observe.

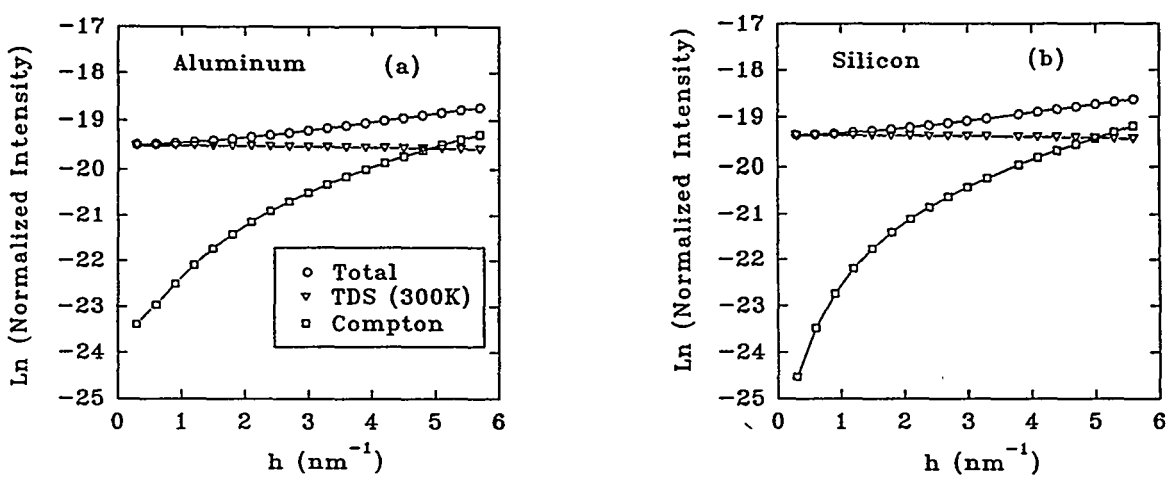

Fig. 24. Theoretical contributions to small-angle x-ray intensity due to incoherent Compton scattering and thermal-diffuse scattering for a) Al and b) Si.

We have done a few experiments where SAXS data were obtained from the pure Al foil and a c-Si wafer as a function of temperature up to about 300°C and the results confirm the expected behavior due to thermal-diffuse scattering (TDS). This is illustrated in Fig. 25 where the experimental and theoretical calculations for c-Si are compared.

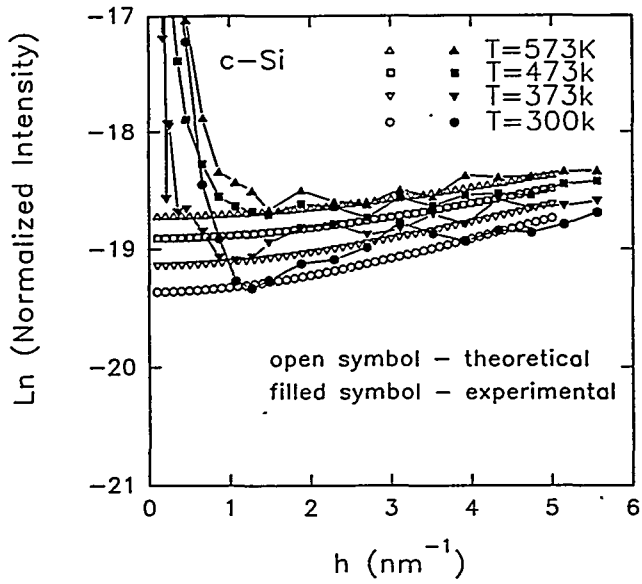

Fig. 25. Experimental and theoretical contributions to small-angle x-ray intensity due to the thermal-diffuse scattering effect.

Based on our improved understanding of these various atomic-scale contributions to the SAXS data, correction procedures are being developed in order to extract the contributions from microvoids and other larger-scale microstrucural features. This is particularly crucial for the more weakly scattering, device-quality materials. We are not aware of any past work on SAXS or small-angle neutron scattering of a-Si-based materials that have even mentioned the Laue monotonic effect, the Compton effect, or the thermal-diffuse contribution, much less detected them.

6.2 Modeling Progress

As demonstrated in some of the data and figures presented so far, significant changes in the SAXS due to tilting the sample relative to the x-ray beam direction have been observed in a-Si:H, a-SiGe:H, a-SiC:H and a-Ge:H films. A qualitative interpretation which is consistent with the typical observation that the SAXS intensity is *reduced* upon tilting is that elongated scattering centers are present with their long axes perpendicular to the film plane. This provides evidence of columnar-like growth in many of the samples. However, as noted above for the ECR films, the SAXS intensity

can also *increase* upon tilting. In order to explain these differences and to extract more quantitative information from the tilt data, a model has been developed based on the following assumptions:

(i) All voids are ellipsoidal in shape but can have various sizes and shapes as prescribed by the minor axis diameters and major/minor axis ratios;

(ii) All voids are oriented with the cylindrical symmetry axis perpendicular to the film plane;

(iii) For a size distribution, up to five minor axis diameters are used and each one can have a different major/minor axis ratio;

(iv) The "infinite slit length" assumption [8,9] is valid for our SAXS system.

Assumption (i) allows a great deal of flexibility in that by varying the ratio one can alter the shape from one of long rods (>>1) to spheres (=1) to thin discs (<<1). Assumption (ii) is quite restrictive but is consistent with columnar growth. We expect to improve this aspect of the model to include a distribution of orientations if problems develop in fitting much of the data. Assumption (iii) implies up to 10 adjustable fitting parameters, but SAXS data at several tilt angles comprises an extensive set of data that must all be fitted consistently and realistically. The last assumption allows us to use the theory for a point x-ray source, modified in a simple analytical way to generate SAXS intensities for our line source apparatus. A refinement of this aspect of the analysis would require a slit-desmearing treatment of our data [8,9], but rough estimates indicate this is relatively unimportant at this stage of our analysis.

The following procedure is used to analyze a set of tilting data:

(i) the SAXS data obtained at zero tilt angle are fitted to obtain up to 5 minor axis sizes. (at this orientation, only the minor axis dimension is relevant);

(ii) Next, a set of SAXS data obtained at some tilt angle are fitted using the minor axis sizes from step (i) and obtain a set of major/minor axis ratios (up to 5, one for each minor axis size);

(iii) additional sets of data measured at other tilting angles, are used to check for a good fit using the parameters obtained from steps (i) and (ii). The parameters are then adjusted to obtain the best overall fit.

This process and the results can be demonstrated for an extensive set of data recently obtained from a film of a-Ge:H deposited at an electrode spacing of 3.2 cm on c-Si (supplied by the Harvard group). Figure 25 shows the SAXS data and theoretical fits for tilt angles of 0, 23, 45, and 60 degrees. Table 13 contains the fit parameters found for each set of data. Note that the 23 degrees angle data show the largest discrepancy. We believe this is due to assumption (ii) above such that for the smallest

tilt angle, a small distribution in axis orientations will cause a stronger effect than at the larger angles. Overall, though, the fits are quite good and the major/minor axis ratios are similar for the various tilts: the predominant void minor diameters are 1.6 and 3 nm and their major/minor axis ratios are consistently about 3 and 6, respectively. In general it appears that the smaller the void, the less the aspect ratio. It will be interesting to determine whether this is a trend among our other samples of a-Si:H, a-SiGe:H and a-SiC:H as well.

The model can readily account for the anomalous tilting SAXS data from the ECR samples noted in section 3.4 by assuming that the major/minor axis ratio is less than unity such that the scattering centers have a disc-like shape. Alternate interpretations are possible, however. For example, rod-like voids that have a preferred orientation within the film plane could also cause the observed effect. Relaxation of assumption (ii) of our model is required to analyze this type of structure but it may be worthwhile in order to try to distinguish between disc-like versus rod-like voids.

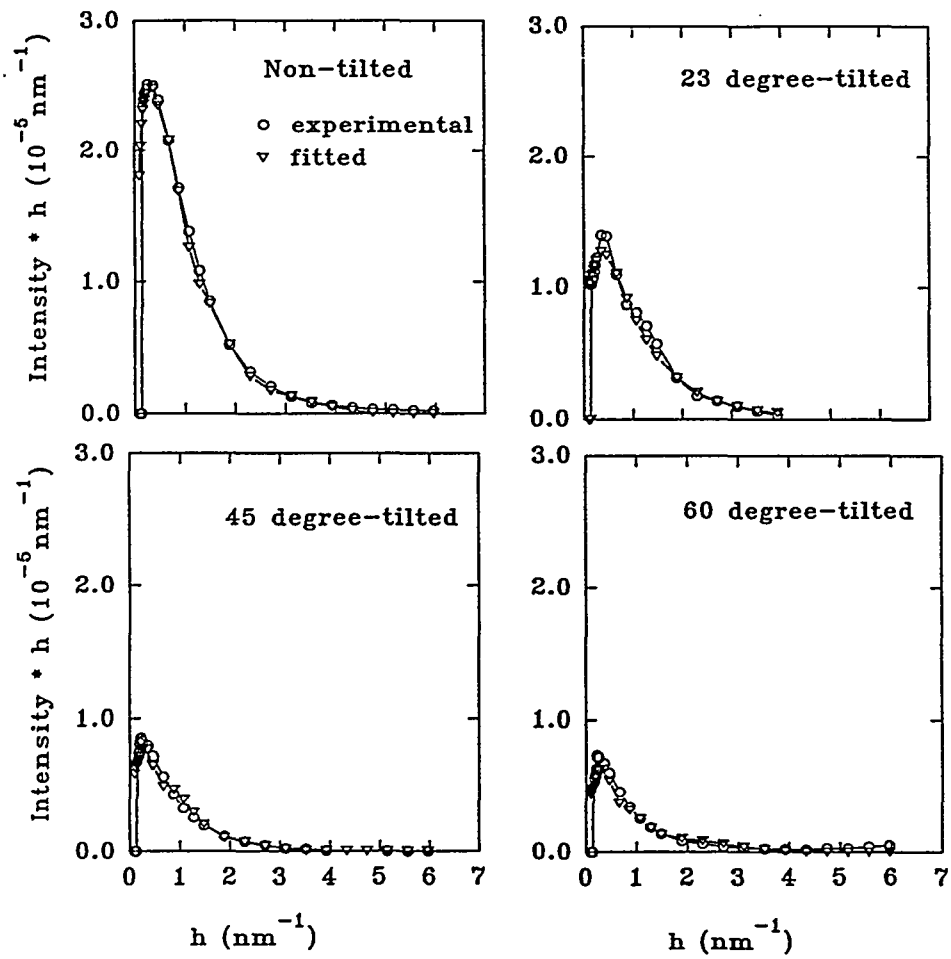

Figure 26. Comparison of SAXS data from a-Ge:H film with theoretical modeling curves based upon distributions of ellipsoidal voids.

Table 13. Fit parameters for the theoretical curves shown in Fig. 26.

Minor Axis Diameter (Å)	Volume Percentage (%)	Major / Minor Axis Ratio Tilt Angles 0°	23°	35°	45°	60°
17	18.9	1	1.5	2.0	2.5	1.5
32	37.6	1	2.5	3.0	2.8	3.0
64	30.7	1	7.5	6.0	6.0	4.3
140	9.5	1	37	14	14	14
280	3.3	1	20	18	18	16

7. INTERDIFFUSION STUDY

The use of Al-foil as a substrate for several structural measurements, including SAXS (e.g., deuteron magnetic resonance, gas evolution, electron spin resonance), raises questions since several reports have shown that at annealing temperatures as low as 200°C, significant amounts of Si can diffuse into Al and induce crystallization. However, all of these studies involve the deposition of Al onto the a-Si without breaking vacuum [26-28]. We have therefore conducted a study of the effects of annealing samples of a-Si:H and a-Ge:H which were deposited onto our SAXS Al-foils (99.999% pure) and other Al substrates. The degree of intermixing at the interface was determined by Auger electron spectroscopy (AES) depth profiling at NREL.

To minimize profiling times, very thin films about 50 nm thick were deposited. Device-quality conditions were used to deposit a-Si:H onto the SAXS Al-foil at Utrecht University. a-Ge:H films were deposited onto the SAXS Al-foil as well as a 5052 Al-based alloy at Harvard University under conditions which led to columnar growth as detected by TEM. Sections of each of these films/substrates were sealed in quartz ampoules under high vacuum and annealed for 6 hours at the following temperatures: 200, 300, 400, 450, and 500°C. For all of the films deposited on the high-purity SAXS Al-foil, little or no interdiffusion was found at or below 400°C. This is in contrast to the results obtained by evaporating Al onto the previously deposited amorphous Si where interdiffusion was noted at 200°C and we attribute the behavior of our films to an oxide barrier present on the Al surfaces. According to AES, an Al-oxide about 15 nm thick is on the SAXS Al-foil.

Annealing at 450°C caused significant interdiffusion for both the a-Si:H and a-Ge:H films and some crystallization was found as detected by Raman spectroscopy. In

the case of the a-Ge:H on the 5052 alloy, interdiffusion occurred at 300°C and a large amount of Mg was detected by AES in the a-Ge:H layer.

We conclude from this study that as long as substrate temperatures are kept below 450°C during deposition (or annealing experiments), there should be little or no interdiffusion or crystallization induced at the SAXS Al-foil/amorphous semiconductor interface. More detailed results from this investigation will be published [29].

8. FUTURE STUDIES

We continue to receive considerable interest in the results of SAXS experiments from several groups that are expert in high-quality film preparation. We therefore expect numerous additional samples during the third year of our contract. NREL will soon be able to provide new material produced by the hotwire method and produced in reconstructed PECVD systems. Additional samples have just been received from USSC, Solarex, Iowa State and U. Illinois. Based on recent communications we expect more samples from Harvard U., U. Neuchatel, Stuttgart U., and Ecole Polytechnique (Paris). Analysis of the films from USSC, Solarex, Iowa State, IEC, and NREL will be given higher priority since they represent samples prepared for analysis by both the Low and High Bandgap Teams formed by the NREL Program Office.

9. ACKNOWLEDGEMENTS

We are extremely grateful to the groups and individuals that have supplied all of the samples and all of the opto-electronic data needed for this research. The graduate student working on this project (Yan Chen) is funded by the Electric Power Research Institute through Technical Agreement RP2824-05. The technical support of NREL in the form of AES and EPMA measurements by Art Nelson, Amy Swartzlander-Franz and Alice Mason is gratefully acknowledged. We are grateful for fruitful discussions with R. Crandall, H. Mahan, H. Branz, B. von Roedern and B. Stafford.

10. REFERENCES

[1] S. Guha, J. Yang, Scott J. Jones, Yan Chen and D.L. Williamson, Appl. Phys. Lett. **61** (1992) 1444.

[2] S.J. Jones, Y. Chen, D.L. Williamson, R. Zedlitz and G. Bauer, Appl. Phys. Lett., June, 1993 [in press].

[3] Scott J. Jones, Yan Chen, D.L. Williamson and G.D. Mooney, Mat. Res. Soc. Symp. Proc. **258** (1992) 229.

[4] S. Muramatsu, T. Shimada, H. Kajiyama, K. Azuma, T. Watanabe, T. Kamiyama

and K. Suzuki, Jpn. J. Appl. Phys. **28** (1989) L1092.

[5] S. Muramatsu, S. Matsubara, T. Watanabe, T. Shimada, T. Kamiyama and K Suzuki, J. Non-Cryst. Solids **150** (1992) 163.

[6] Yan Chen, S.J. Jones, D.L. Williamson, S. Yang, N. Maley and J.R. Abelson, Mat. Res. Soc. Symp. Proc. **258** (1992) 311.

[7] A.H. Mahan, D.L. Williamson, B.P. Nelson and R.S. Crandall, Solar Cells **27** (1989) 465.

[8] A. Guinier and G. Fournet, *Small Angle Scattering of X-rays* (Wiley, New York, 1955)

[9] *Small Angle X-ray Scattering,* O. Glatter and O. Kratky, eds. (Academic, New York, 1982)

[10] D.L. Williamson, A.H. Mahan, B.P. Nelson, and R.S. Crandall, Appl. Phys. Lett. **55** (1989) 783.

[11] D.L. Williamson, A.H. Mahan, B.P. Nelson and R.S. Crandall, J. Non-Cryst. Solids **114** (1989) 226.

[12] A.H. Mahan, D.L. Williamson, B.P. Nelson and R.S. Crandall, Phys. Rev. **B40** (1989) 12024.

[13] A.H. Mahan, Y. Chen, D.L. Williamson and G.D. Mooney, J. Non-Cryst. Solids **137&138** (1991) 65.

[14] S. Guha, Final Report, SERI/TP-211-3918, National Renewable Energy Laboratory, Golden, Colorado, 1990.

[15] A. Matsuda, S. Mashima, K. Hasezaki, A. Suzuki, S. Yamasaki and P.J. McElheny, Appl. Phys. Lett. **58** (1991) 2494.

[16] A.Shah, J. Dutta, N. Wyrsch, K. Prasad, H. Curtins, F. Finger, A. Howling and Ch. Hollenstein , Mat. Res. Soc. Symp. Proc. **258** (1992) 15.

[17] U. Kroll, F.Finger, J. Dutta, H. Keppner, A. Shah, A. Howling, J.-L-Dorier and Ch. Hollenstein, Mat. Res. Soc. Symp. Proc. **258** (1992) 135.

[18] M.B. Schubert, H.-D. Mohring, E. Lotter and G.H. Bauer, IEEE Trans. Electr. Devices **36** (1989) 2863.

[19] K.D. Mackenzie, J.R. Eggert, D.J. Leopold, Y.-M. Li, S. Lin and W. Paul, Phys. Rev. **B31** (1985) 2198.

[20] H.J. Leamy, G.H. Gilmer and A.G. Dirks, *Current Topics in Materials Science*, Vol. 6, ed. E. Kaldis (North Holland, Amsterdam, 1980) p.309.

[21] L.H. Schwartz and J.B. Cohen, *Diffraction from Materials* (Springer-Verlag, Heidelberg, 1987) p.232.

[22] P. Wickbolt, S.J. Jones, F.C. Marques, D. Pang, W.A. Turner, A.E. Wetsel, W.

Paul and J.H. Chen, Phil. Mag. B **64** (1991) 655.

[23] P. Wickbolt, Ph.D. Thesis, Harvard University (1993).

[24] S.J. Jones, Ph.D. Thesis, Harvard University (1991).

[25] S.J. Jones, Y. Chen, D.L. Williamson, P. Wickbolt, D. Pang, A.E. Wetsel, W. Paul and J.H. Chen [in preparation].

[26] W.B. Berry, K.A. Emery, A.B. Swartzlander and A.J. Nelson, Proc. 20th IEEE Photovol. Spec. Conf. **1** (1988) 262.

[27] V.O. Abramov, A.S. Avilov, A.N. Belokonov, Y.A. Zarif'yants, V.A. Milyaev and A.V. Shirkov, Sov. Phys. Semicond. **19** (1985) 224.

[28] S. Ishihara, M. Kitagawa and T. Hirao, J. Appl. Phys. **62** (1987) 837.

[29] S.J. Jones, A.B. Swartzlander-Franz, Y. Chen and D.L. Williamson, Mat. Res. Soc. Symp. Proc. (Spring, 1993, in press).

REPORT DOCUMENTATION PAGE

Form Approved
OMB NO. 0704-0188

Public reporting burden for this collection of information is estimated to average 1 hour per response, including the time for reviewing instructions, searching existing data sources, gathering and maintaining the data needed, and completing and reviewing the collection of information. Send comments regarding this burden estimate or any other aspect of this collection of information, including suggestions for reducing this burden, to Washington Headquarters Services, Directorate for Information Operations and Reports, 1215 Jefferson Davis Highway, Suite 1204, Arlington, VA 22202-4302, and to the Office of Management and Budget, Paperwork Reduction Project (0704-0188), Washington, DC 20503.

1. AGENCY USE ONLY (Leave blank)	2. REPORT DATE	3. REPORT TYPE AND DATES COVERED
	May 1994	Subcontract Report — 1 February 1992 - 31 January 1993

4. TITLE AND SUBTITLE

Small-Angle X-Ray Scattering Studies of Microvoids in Amorphous Silicon-Based Semiconductors

5. FUNDING NUMBERS

C: XG-1-10063-3

TA: PV431101

6. AUTHOR(S)

D.L. Williamson, S.J. Jones, Y. Chen

7. PERFORMING ORGANIZATION NAME(S) AND ADDRESS(ES)

Colorado School of Mines
Department of Physics
Golden, Colorado 80401

8. PERFORMING ORGANIZATION REPORT NUMBER

9. SPONSORING/MONITORING AGENCY NAME(S) AND ADDRESS(ES)

National Renewable Energy Laboratory
1617 Cole Blvd.
Golden, CO 80401-3393

10. SPONSORING/MONITORING AGENCY REPORT NUMBER

TP-411-6612

DE94011815

11. SUPPLEMENTARY NOTES

NREL Technical Monitor: A. H. Mahan

12a. DISTRIBUTION/AVAILABILITY STATEMENT

12b. DISTRIBUTION CODE

UC-271

13. ABSTRACT *(Maximum 200 words)*

This report describes work to provide new details of the microstructure for the size scale from about 1 nm to 30 nm in high-quality a-Si:H and related alloys prepared by current state-of-the-art deposition methods as well as by new and emerging deposition technologies to help determine the role of microvoids and other density fluctuations in controlling the opto-electronic properties. The objectives are to determine whether the presence of microstructure as detected by small-angle X-ray scattering (SAXS) (1) limits the photovoltaic (PV) properties of device-quality a-Si:H; (2) plays a role in determing the photostability of a-Si:H; and (3) is responsible for degradation of the PV properties due to alloying with Ge, C, and other constituents. We collaborated with several groups that can supply relevant systematic sets of samples and the associated opto-electronic data to help address these issues. The project also included developing a method to standardize the procedures, minimize substrate influences, and implement improved data reduction and modeling methodology.

14. SUBJECT TERMS

amorphous silicon ; semiconductors ; small-angle X-ray scattering ; photovoltaics ; solar cells

15. NUMBER OF PAGES
50

16. PRICE CODE
A03

17. SECURITY CLASSIFICATION OF REPORT	18. SECURITY CLASSIFICATION OF THIS PAGE	19. SECURITY CLASSIFICATION OF ABSTRACT	20. LIMITATION OF ABSTRACT
Unclassified	Unclassified	Unclassified	UL